AWARD NUMBER: W81XWH-21-1-0138

TITLE: Closed-Loop Recording-Stimulation System for Accelerating Recovery After Musculoskeletal Injury

PRINCIPAL INVESTIGATOR: Yakovenko, Sergiy

CONTRACTING ORGANIZATION: West Virginia University, Morgantown, WV

REPORT DATE: March 2022

TYPE OF REPORT: Annual

PREPARED FOR: U.S. Army Medical Research and Development Command
Fort Detrick, Maryland 21702-5012

DISTRIBUTION STATEMENT: Approved for Public Release;
Distribution Unlimited

REPORT DOCUMENTATION PAGE

Form Approved
OMB No. 0704-0188

1. REPORT DATE	2. REPORT TYPE	3. DATES COVERED
March 2022	Annual	15Feb2021 – 14Feb2022

4. TITLE AND SUBTITLE

Closed-Loop Recording-Stimulation System for Accelerating Recovery After Musculoskeletal Injury

5a. CONTRACT NUMBER
W81XWH-21-1-0138

5b. GRANT NUMBER
DM190880

5c. PROGRAM ELEMENT NUMBER

6. AUTHOR(S)
Yakovenko, Sergiy

E-Mail: seyakovenko@hsc.wvu.edu

5d. PROJECT NUMBER
0011574052

5e. TASK NUMBER

5f. WORK UNIT NUMBER

7. PERFORMING ORGANIZATION NAME(S) AND ADDRESS(ES)
WEST VIRGINIA UNIVERSITY RESEARCH CORPOR
ALAN B MARTIN

886 CHESTNUT RIDGE
MORGANTOWN WV 26506-2742

8. PERFORMING ORGANIZATION REPORT NUMBER

9. SPONSORING / MONITORING AGENCY NAME(S) AND ADDRESS(ES)

U.S. Army Medical Research and Development Command
Fort Detrick, Maryland 21702-5012

10. SPONSOR/MONITOR'S ACRONYM(S)

11. SPONSOR/MONITOR'S REPORT NUMBER(S)

12. DISTRIBUTION / AVAILABILITY STATEMENT

Approved for Public Release; Distribution Unlimited

13. SUPPLEMENTARY NOTES

14. ABSTRACT

Combat and training related arm injuries often paralyze one or more muscles and impair movement. Nerve damage leads to poorly functioning muscles, which degenerate overtime. In this proposal, we will develop non-invasive technology that will help prevent muscle wasting, exercise functioning muscles, and speed up recovery. This technology addresses the following Focus Areas: 1) accurate diagnosis of neuromusculoskeletal injuries; 2) developing objective support tools to enable assessment of function and performance during treatment; 3) optimization and acceleration of the recovery and restoring Warfighter performance after limb trauma or loss.

Mathematical models of anatomy capture how muscles cause motion in the presence of external forces, such as gravity. Unfortunately, considering only motion without calculating the forces causing this motion, as often done in clinical practice, is insufficient for the understanding of how well the arm functions or what goes wrong when it does not function as needed. This is because even in a seemingly relaxed arm, muscles are often co-activated so that their forces counterbalance each other around the joints. Thus, muscles do a lot with no visible motion. Therefore, the critical need is to use the information from detailed mathematical models of muscle forces and of their interaction with the forces in the world in the rehabilitation of injured muscles.

The long-term goal of this project is to develop automated diagnostic and treatment systems for the assessment and rehabilitation of movement deficits after arm injury. The focus of this proposal is to develop the technology for predicting intended motion from the activity of undamaged muscles and inducing contractions in paralyzed or underused muscles using a high-density electromyographic (hdEMG) technology for neuromuscular electrical stimulation (ES). We have accomplished the first aim to improve existing algorithms and devices for hdEMG-ES to predict and intervene in the motion of the forearm using the activity of upper arm muscles and vice versa. We have improved the model of the arm anatomy to better represent the human arm. We have also developed virtual reality tasks and built a system with a wearable sleeve that can record ongoing muscle activity from the forearm. We have collected a pilot dataset to be used for algorithm development. We have started the development of the wearable sleeve that can stimulate muscles under the control of the model arm. These accomplishments will enable achieving the second aim to evaluate the system performance, including in participants with amputations and denervated muscles. This will show the feasibility of the approach to maintain shoulder muscle health in amputees by preventing shoulder muscle weakening and to maintain the health of denervated muscles.

The outcomes of this research will translate current scientific knowledge into objective diagnostic tools. The new designs of an ES-based, exercise-based, or robot-assisted rehabilitation techniques will be enabled by the technology developed in this project. Patient progress and warfighter performance can be objectively monitored with the model and

i t l t k

15. SUBJECT TERMS

None listed.

16. SECURITY CLASSIFICATION OF:			**17. LIMITATION OF ABSTRACT**	**18. NUMBER OF PAGES**	**19a. NAME OF RESPONSIBLE PERSON**
					USAMRDC
a. REPORT	**b. ABSTRACT**	**c. THIS PAGE**		30	**19b. TELEPHONE NUMBER** *(include area code)*
Unclassified	Unclassified	Unclassified	Unclassified		

Table of Contents

1. Introduction

Musculoskeletal injuries are a significant threat to combat readiness with 2.3 injuries occurring per soldier over the extent of a year and with close to half of injuries unreported (Smith et al., 2016) and 9.5% of hospitalizations leading to disability discharge (Lincoln et al., 2002). Combat and training related arm injuries often paralyze one or more muscles and impair movement. Nerve damage leads to secondary effects such as the degeneration of denervated muscles and maladaptive nonfunctional neural plasticity, which limits the speed of recovery. In this proposal, we will develop technology towards overcoming maladaptations by using high-density electromyography and electrical stimulation (hdEMG-ES) driven by musculoskeletal dynamic (MSD) modeling to enforce functional recovery and maintenance of denervated muscle tissue. The mathematical framework of MSD models is necessary for stimulating patterns that capture how muscles generate motion in the presence of external forces, such as gravity, given the individual arm anatomy and inertia. Unfortunately, considering only kinematic motion, as often done in clinical practice, is insufficient for the understanding of joint stability and overall limb function. This is because in a seemingly relaxed arm muscles are often co-activated so that their forces counterbalance each other around the joints. Thus, significant muscle loading occurs in stabilizing tasks with no overall motion, yet, supporting the limb joints against external perturbations, e.g., heavy objects, or expected interaction forces from other segments due to voluntary motion. The critical need is to rehabilitate injured muscles with the use of embedded co-activation control signals and healthy dynamics. The long-term goal of this project is to develop automated diagnostic and interventional systems for the assessment and rehabilitation of motor function after musculoskeletal injury. The focus of this proposal is to develop the technology for quantifying intended voluntary motion from the activity of undamaged muscles and inducing congruent activity of paralyzed muscles using high-density electrode arrays.

2. Keywords

Electrical stimulation, motion capture, electromyography, motor control, rehabilitation

3. Accomplishments

What were the major goals of the project?

The main goal of this project is to develop automated diagnostic and interventional systems for the assessment and rehabilitation of motor function after musculoskeletal injury. The focus of this proposal is to develop the technology for quantifying intended voluntary motion from the activity of undamaged muscles and inducing congruent activity of paralyzed muscles using high-density electrode arrays.

Specific Aim 1: Expand existing algorithms and devices for hdEMG-ES systems to predict and intervene in the motion of distal segments using activity of proximal arm muscles	**Original Timeline** Months	**New Timeline** Months	**Progress, %**
Major Task 1.1: Expansion of device capabilities			
Subtask 1.1.1: Expand the MSD model to include shoulder degrees of freedom	1-3	1-12	*100*
Subtask 1.1.2: Development of experimental setup with VR tasks of arm function	1-3	1-3	100
Subtask 1.1.3: Design and build a flexible electrode array for hdEMG-ES of the arm and increase of channel count for multichannel recording and stimulation	3-6	3-24	*100*
Milestone #1: Submitted IP disclosure on the design of multichannel recording-stimulation electrode array	6-7	*12*	DONE
Major Task 1.2: Obtaining normative data on high-density EMG			
Subtask 1.2.1: HRPO regulatory review of hdEMG recording studies	1-3	1-3	*100*
Subtask 1.2.2: Recruit healthy participants and conduct experiments with VR tasks recording hdEMG and motion capture	3-9	3-9	50
Subtask 1.2.3: Develop decoder to predict distal muscle activity from proximal hdEMG and disseminate results	5-12	5-18	*50*

Subtask 1.2.4: Develop an algorithm to predict the changes in proximal muscle activity due to motion of distal segments using MSD model	5-12	5-18	*30*
Milestone #2: Obtain HRPO approval for recording studies	2-3	6	*DONE*
Milestone #3: Submitted manuscript on the use of MSD model to decode wrist and hand motion from the hdEMG of muscles spanning shoulder and elbow	11-12	16-17	
Milestone #4: Submitted manuscript on the use of MSD model to decode the muscle activity due to the load at the shoulder from the motion of the forearm	11-12	18-19	

What was accomplished under these goals?

Major activities

Specific objectives

The focus of Q1 was on the initiation of our team tasks that includes: 1) the support of submission to HRPO regulatory review, 2) the initial development of hardware and software to support the experimental work with human subjects. The focus of Q2 was on the implementation of experimental procedures that includes: 1) development of virtual tasks, 2) the initial development of hardware and data collection pipelines to support the experimental work with human subjects. The focus of Q3 was on the continued implementation of experimental procedures to conduct experimental work with human subjects that includes: 1) the testing of the virtual and real-world tasks with data collection pipelines and hardware integration, 2) the testing of the quality of data obtained with the custom-made array. The focus of Q4 was on 1) hardware integration for EMG recordings and the electrical stimulation with the custom-made array and 2) collecting normative dataset.

Significant results

Specific Aim 1: Expand existing algorithms and devices for hdEMG-ES systems to predict and intervene in the motion of distal segments using activity of proximal arm muscles

Major Task 1.1: Expansion of device capabilities

Subtask 1.1.1: Expand the MSD model to include shoulder degrees of freedom

MSD model with improved shoulder dynamics

The model of arm and hand has been substantially improved through the development of simplified models of pronation supination (Fig.5), robust and consistent simulation model of forward and inverse dynamics (Fig.4), generation of custom arm and hand movements, and the addition of shoulder muscles (Fig.1-3). The validation of 11 of 19 shoulder muscles has been completed (Subtask 1.1.1).

We have expanded upon a previously published model (Saul et al., 2015) to convert the degrees of freedom (DOFs) of the shoulder to Euler angles. The Euler-based shoulder coordinate system will enable the comparison of muscle moment arms to published values. The scapular and clavicular motion has been described as a function of humerus elevation:

$$[\theta_{scapula}, \theta_{clavicle}] = f(\theta_{humerus})$$

where *θ_scapula* is a vector of Euler angles describing the orientation of the scapular relative to the trunk; *θ_clavicle* is a vector of Euler angles describing the orientation of the clavicle relative to the trunk; and *θ_humerus* is a vector of Euler angles of the glenohumeral joint describing the orientation of the humerus relative to the trunk.

We evaluated the anatomical accuracy of our musculoskeletal model by comparing simulated musculotendon moment arms with published measurements from the literature (Ackland et al., 2008; Boots et al., 2020; Folgado et al., 2013; Quental et al., 2012). Moment arms were simulated using the OpenSim software. A physiological coordinate system was added to the shoulder joint to allow comparison of simulated moment arms to values measured in the literature (see Shoulder DOFs). Each DOF was permuted across the defined range of motion uniformly at a sampling rate of 9 postures per DOF. Musculotendon moment arms were acquired for each DOF that a muscle crossed for each iteration (Fig. 1). Moment arm profiles were then interpolated using

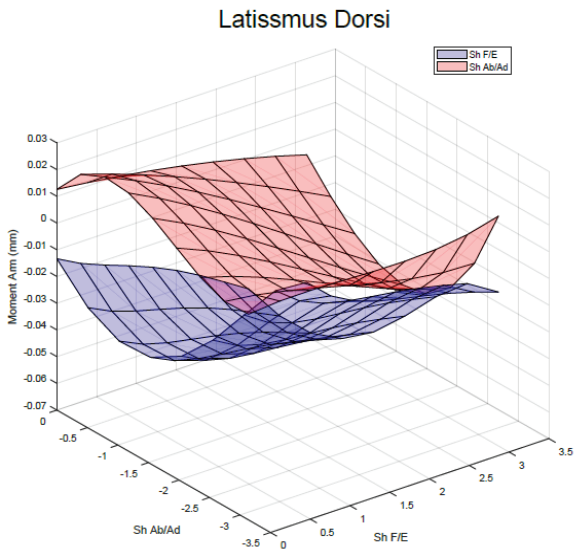

Figure 1: Example of changes in moment arms for latissimus dorsi muscle as a function of posture. Sh is abbreviation for shoulder, F/E is abbreviation for flexion/extension DOF; Ab/Ad is abbreviation for abduction/adduction DOF.

a polynomial fitting procedure described in Sobinov, 2019 (Sobinov et al., 2019). These polynomials approximated the musculotendon moment arms as a function of model posture.

To validate the physiological accuracy, we evaluated the polynomial approximations using the same postures that were used during moment arm measurements in the literature (Ackland et al., 2008; Folgado et al., 2013; Quental et al., 2012). The simulated moment arms were then compared to the published measurements by calculating the root mean square (RMS) normalized to the range of motion. Additionally, moment arm profiles were qualitatively assessed by classifying discordant moment arm profiles based upon the error that was induced. Boots et al, 2020 provides a more comprehensive description of the validation procedure along with results for the elbow, wrist, and hand (Boots et al., 2020). The remainder of this chapter will describe the validation of muscles spanning the shoulder.

To validate the musculotendon paths of shoulder muscles to values published in the literature, the shoulder coordinates were first transformed into the Euler coordinates (flexion/extension, abduction/adduction, internal/external rotation). The simulated moment arms were acquired as described above using the non-Euler coordinate system to articulate the joint. The matrix of postures was then transformed into the Euler defined coordinate system prior to polynomial fitting. This transformation was achieved by first converting the model's axis-angle representation into a quaternion representation. The coordinates were then rotated using the Hamilton product.

$$q' = q_1 q_2$$

Here q_1 and q_2 are the first and second rotation respectively. Finally, the newly rotated quaternion coordinate was converted into Euler angles corresponding to flexion/extension, abduction/adduction, and internal/external rotation.

Moment arm profiles were plotted relative to the reference dataset created from the published values. Then, the differences between published and simulated moment arm values were iteratively changed by modifying muscle path in OpenSim to reduce the discrepancy. The development and validation of shoulder muscle moment arms is ongoing, but the current status of the model is shown in Fig. 2. Moment arms around internal and external rotation are not included as experimental measurements have not yet been found in the literature.

The validated musculotendon moment arms were analyzed using the hierarchical clustering of HVE previously described in Methods. Shoulder muscle moment arms cluster into two distinct clusters based upon their action around each DOF (Fig. 3). This result is consistent with moment arm relationships at the elbow, wrist, and hand (Boots et al., 2020). The correlation of muscle moment arms with similar function means that moment arms change together in different postures, they do so as a functional group, e.g. if the moment arm of the anterior deltoid in increasing so too are the moment arms of other shoulder flexors. It is noteworthy that these clusters are not conserved across DOF, i.e. a shoulder flexor is not always an abductor nor is a shoulder extensor. Further model validation during the following tasks will confirm the robustness of these relationships. The outcomes of this analysis will be incorporated into the controller for stimulation in future tasks.

Subtask 1.1.1a: Simbody model development

Quarantine restrictions delayed our efforts in the collection of experimental data and its integration with the models. To mitigate this, we have further expanded MSD model capabilities by developing an equivalent model of arm and hand in Simulink (Fig. 4). The shoulder is modeled as a 3-DOF spherical joint with cardan Euler angles matching those implemented in OpenSim model described above. The rest of the DOFs and the inertial parameters of the model also match those of OpenSim model. This model will be used to create an extensive simulated movement dataset for controller development and testing as described below in Subtask 1.1.1b.

Human hand pronation-supination movement is accomplished by the movement of the radius and ulna bones relative to each other via the proximal and distal radioulnar joints, each with multiple degrees of freedom (DOFs). Here, we developed two simplified models in Simulink (MathWorks, Inc) to simulate these movements within a 20 DOF model of the hand and forearm. The pronation/supination DOF was implemented as a single rotation joint either within the forearm segment or separating proximal and distal parts of the forearm segment (Fig. 5). Torques produced by the inverse dynamic simulations in OpenSim with the anatomical architecture that included the forearm (Saul et al., 2015) were used as the "gold standard" to evaluate the two simple models. Both Simulink models matched the OpenSim model in all inertial and morphometric parameters except for the forearm segment and pronation/supination joint.

To validate the model simplifications, multiple hand movements were simulated with bell-shaped velocity profiles to mimic characteristic point-to-point movements. We computed applied joint torques for all models using inverse dynamics driven by angular kinematics of each of the 65 movements. The OpenSim and Simulink joint torques were compared by calculating root-mean-squared-error (RMSE) for each DOF, for all movements. The RMSE values were normalized to the torque range of the OpenSim model per DOF per movement.

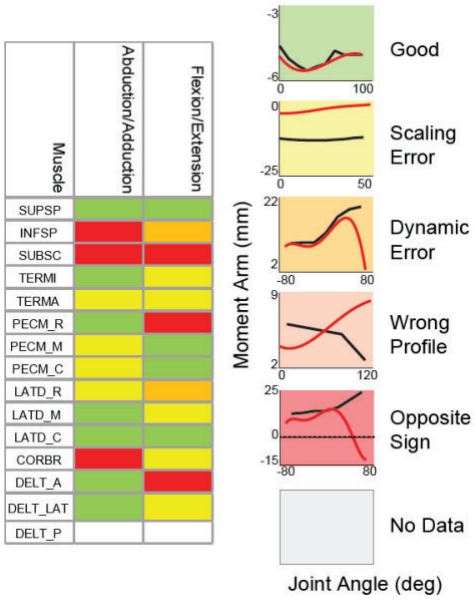

Figure 2: Qualitative metric of moment arm quality. A list of all muscles that span the shoulder that are included in the model are in the table on the left. The colors indicate the qualitative metrics that is summarized in text.

Despite known difficulties in obtaining consistent solutions across platforms (Wagner et al., 2013), we have achieved matching inverse simulation results between OpenSim and Simulink models. For example, even the model with a simplified pronation/supination joint in a solid, cylindrical forearm produced joint torques that closely matched the OpenSim model with separate radius and ulna segments (Fig. 5A). These errors were mostly below 10% of peak-to-peak torques across all simulated joints and movements, with pronation/supination being the most adversely affected DOF. Our results have shown that a simple 1-DOF pronation/supination joint at the elbow can provide reasonable approximations for biomedical applications. We intend to use this solution in combination with the approximations of moment arm dependency on posture as were previously described (Sobinov et al., 2020).

The segmented forearm model (Fig. 5C) performed with high precision across all tested movements. The errors were within perceived joint positional errors in previous human psychometric studies (Gritsenko et al., 2007). The non-uniform proximal and distal cylindrical segments closely matched the moments of inertia of the

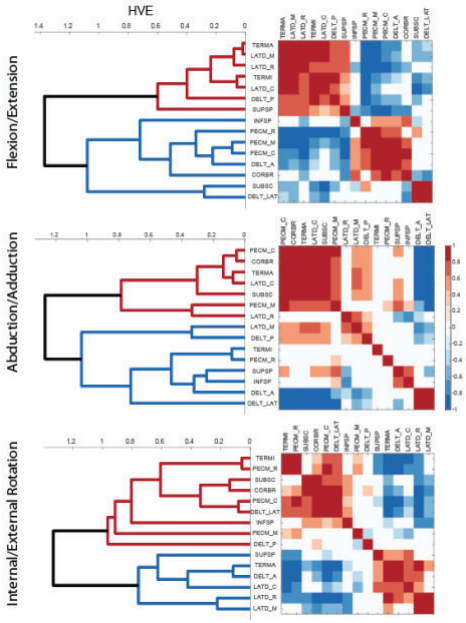

Figure 3: Hierarchical clustering of shoulder muscle moment arms. Correlation matrices of moment arm profiles across multiple postures of the shoulder are shown on the right, red squares denoting positive correlations (synergistic relationship between corresponding muscles) and blue squares denoting negative correlations (antagonistic relationship between corresponding muscles). HVE stands for hierarchical variance explained, a metric of similarity between profiles of moment arms for different muscles derived from the correlation matrix. **This analysis shows which shoulder muscles act together to produce a single action.**

radius segment rotating about the ulna segment. The errors between OpenSim and Simulink models were: 1) pronation/supination torque mean RMSE = 0.04 [normalized units (nu)], interquartile range of 0.02 - 0.06 [nu] for solid forearm model, and 2) RMSE = 0.01 [nu], interquartile range of 0.01 - 0.03 [nu] for split forearm model. The split forearm model simulates pronation/supination as a single DOF about an axis parallel to both compartments of the forearm, providing the benefit of a simplified dynamic simulation. This result has direct implications for our development by simplifying dynamic simulations with minimal reduction in accuracy.

1.1.1b. Dynamic dataset

We used the Simulink model to generate a comprehensive dynamic description of physiological movement that includes both joint kinematics and kinetics. We then used these datasets in the high-fidelity approximated dynamic transformations. All possible movements between the selected postures were created using the bell-shaped velocity constraint with zero starting and final velocities. The grid was defined by 3x3x3 postures spanning positions on both sides of the body's midline and covering the central area of space between shoulders. The total number of movements, defined by the combinatorial combination $C(n,k) = \frac{n!}{k!(n-k)!}$, where *n* is the number of postures and *k* is the number of postures in a selection (*k*=2), was 351. To evaluate the impact of varied dynamics during each movement, the maximum velocity was defined by a gaussian and three movement durations (0.5, 1.0, 2.0 s). This dataset captured a diverse subset of dynamic repertoire (reaching, defense, and manipulation) typically examined in primate research of limb control (Graziano, 2016). The resulting data was organized as the structure containing *[x,v,a,tau],* where x is the vector of joint angles, v and a are its angular velocity and acceleration, and tau is the joint torque. For 23 DOF model, each vector contained 69 signals sampled at 10 kHz. This dataset was split into training, validation, and testing subsets of 100 ms batches constituting respectively 70%, 15%, and 15% of the full dataset. **The test data was not used in training, and the performance represented the expected physical transformations within the processing pipeline.**

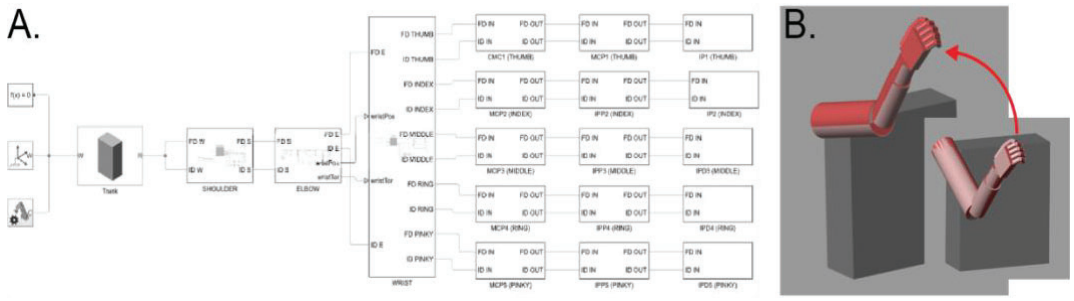

Figure 4. Dynamical model for inverse and forward (ID-FD) simulations of arm and hand movement. A. The structural model implementation in Simulink. **B.** The model visualization is driven by kinematics (light red) with simultaneous forward dynamics (dark red). The two models correspond to the starting and final model postures. The difference in two superimposed structures indicate the accumulated numerical error in the simulations, typically below 1% of range of motion for each DOF. **The use of simultaneous ID-FD simulations validates the high quality of simulated dynamics.**

Subtask 1.1.2. Development of experimental setup with VR tasks of arm function

Unreal Engine 4.26 was used to develop the virtual environment for the Box and Block Test (BBT). First, a table was created and placed in the virtual environment. Then, the box assembly for the BBT was constructed according to the dimensions in Mathiowetz et al., 1985. The box assembly was placed on the table in VR and twenty blocks were placed in the box assembly, five of each color – red, blue, green, and yellow. The texture of the table was set to dark wood, while the box assembly was set to light colored wood to match the real-world appearance. Then, real-time hand visualization and motion capture was enabled using the Oculus Hand Controllers (Fig. 6). This development was guided by a YouTube tutorial and modified to utilize the index finger – thumb distance for picking up the blocks, rather than the fingertip – palm of hand distance. Object interaction was developed, and we were able to pick up the blocks and perform the action of the BBT in the virtual environment.

Finally, a connection was established between Matlab and Unreal to facilitate real-time data export from hand positions in Unreal into the Matlab workspace for further analysis. Connection was verified with "Hello Matlab" and "Hello Unreal" prompts on the corresponding screens.

Throughout the reporting period, we refined the VR experimental setup to reduce inter-subject variability. We added a calibration procedure to standardize the placement of the virtual objects across subjects during the virtual Box Block Test (BBT) developed in the previous quarter. We developed scripts to place the virtual table at a distance from the subject proportional to the length of his/her segment from elbow to center of the hand, and a height proportional to the distance from the floor to the elbow (Fig. 7). The same procedures are followed during a real-world BBT.

The second procedure for standardizing the virtual BBT is to present a single block at a time to the subject so that the movements to reach and pick up the block have the same initial conditions across repetitions of block manipulation and across subjects. The one block will appear at the same position on the table and the target location will be marked on the other side of the box assembly (Fig. 8). Once the participant transfers the block across the barrier and drops it on the target (Fig. 8, black circle with red X), the target will shift to the opposite side of the box assembly. This sequence will repeat 20 times and will be closely matched to the real-world BBT procedure.

These modifications to the virtual and real-world BBT will reduce both intra-subject and inter-subject variability in motion capture and electromyographic (EMG) data.

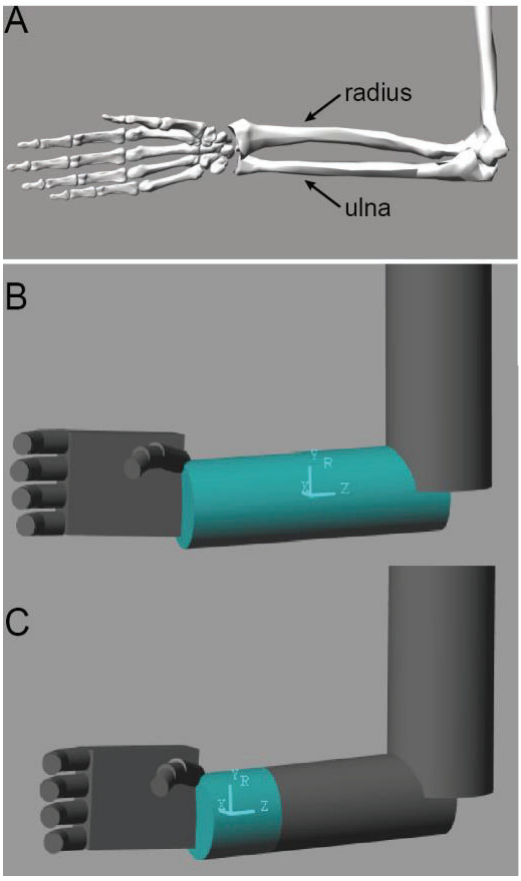

Figure 5: Simplifying hand models. **A.** OpenSim model illustrating the anatomy of the forearm and hand segments. The pronation/supination is accomplished by radius rotating around the ulna. **B.** Simplified Simulink model with a single forearm segment. Axes show a local coordinate system of the forearm segment. The pronation/supination degree of freedom is the rotation of the forearm segment around the long axis (Z). **C.** Simplified Simulink model with segmented forearm. Axes show a local coordinate system of the distal forearm segment. The pronation/supination degree of freedom is the rotation of the distal forearm segment around the Z axis.

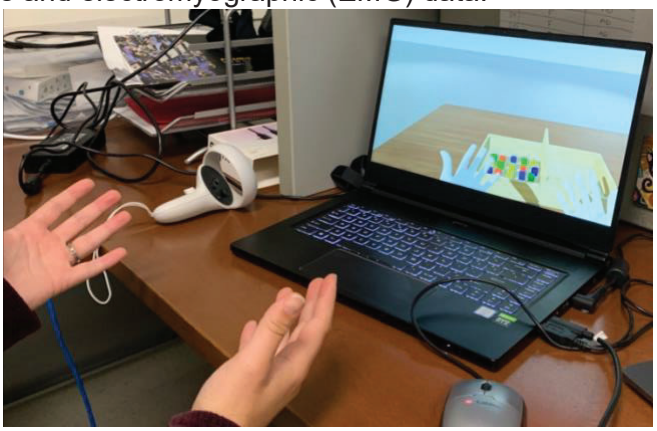

Figure 6. Establishing hand tracking in VR with the Oculus Quest 2

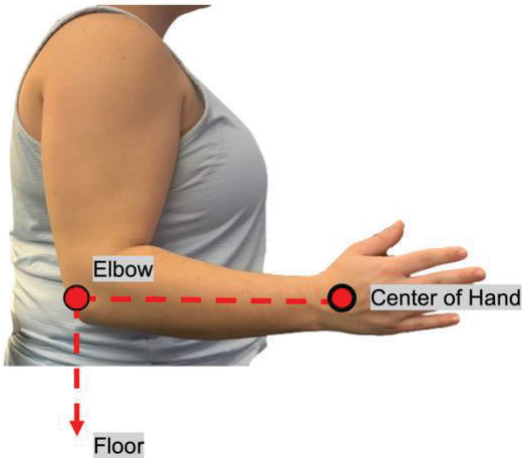

Figure 7. Lengths and distances measured to calibrate the VR setup to individual body dimensions and position relative to world reference frame.

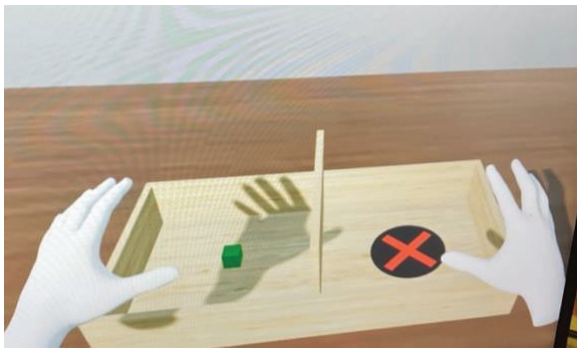

Figure 8. Box and Block Test with one block appearing and target location for dropping

Subtask 1.1.3: Design and build a flexible electrode array for hdEMG-ES of the arm and increase of channel count for multichannel recording and stimulation

High-density array design and manufacturing procedures:

The array will be manufactured from commercially available off-the-shelf components for transcutaneous electrical stimulation, which is a procedure commonly used to reduce pain, muscle spasms, improve blood flow, or reduce spasticity among other benefits. The main components of the array are leads with connectors and electrode pads.

Leads with connectors: We will use different types of leads with connectors specific to recording or stimulation hardware. For recording, insulated stainless-steel wire (conductivity = $0.145*10^7$ S/m) leads soldered to the Omnetics (Omnetics Connector Corporation) connector for interfacing with Grapevine (Ripple, see hardware specs in Appendix A for Grapevine User Manual) will be purchased pre-made from Omnetics Connector Corporation. For stimulation, insulated copper wire soldered to D188-09 1.5mm touch-proof connector will be purchased pre-made from Digitimer (see hardware specs in Optional Accessories for Digitimer D188 Manual). Both types of leads will be attached to the same types of electrode pads described in the next paragraph. To accomplish that, each wire will be stripped from insulation to expose 0.5 cm conductor at the tip and soldered to the gold-plated 1.5mm male connector. These will plug into the matching female connector on the electrode pad.

Electrode pad: The electrode pad will consist of insulating frame, conductive electrode, and skin interface layer. The insulating frame will be manufactured from thermoplastic polyurethane (TPU), which is a type of elastomer used in 3D printing filaments with advantageous properties such as elasticity and resistance to abrasion. This material is between hard plastic and soft silicon showing long-term structural stability over other flexible filaments used in 3D printing (Lambertz et al. 2015). The conductive electrodes will be inserted into the TPU-based insulation frame to create a robust array assembly. The standard silver/silver chloride or nickel-plated brass electrodes 0.5 - 1 cm in diameter will be purchased from manufacturers or distributors (for example, Bio Medical Instruments). The smaller electrodes will be used for recordings, while the larger for stimulation. After insertion into the insulation frame, each electrode will be soldered to the gold-plated 1.5mm female connector. Each of these will plug into the matching male connector on a lead for either recording or stimulation. After that, the surface of each electrode will be covered with an adhesive hydrogel layer purchased from distributors (for example, Walmart, Amazon). This will provide safe skin interface for transcutaneous electrical stimulation based on the published recommendations for electrode design (Keller and Kuhn 2008).

The quality of the assembly will be tested using a multimeter. Resistance of the electrode with lead and connector assembly is the indicator of the quality of electromyographic signals during recording and of the predictability of transcutaneous current during stimulation. The resistance of leads attached to small electrodes for recording will need to be less than 1 KOhm. The resistance of leads attached to the large electrodes for stimulation will need to be between 1 - 50 Ohm.

We conducted testing of the manufacturing process developed in the previous quater. We compared the main design of the electrode assembly with small electrode pads (circular electrodes) described above for EMG recordings to a simplified design of a lead soldered to a male connector without the electrode pad (pin electrode). We also collected data using “electrode-less” EMG wire to set a baseline signal as well as ensure the quality of our manufacturing process (Fig. 9).

Figure 9: High-density electromyography (hdEMG) array testing. Circular electrodes (left), pin electrodes (middle), bare wire (right).

To test these electrodes, we placed two of each type of electrodes parallel to the direction of the muscle fibers on a subject’s right bicep muscle. We chose the large bicep muscle because all three pairs of electrodes can be placed on it and pick up isolated myoelectric signals during elbow flexion movements driven by biceps contractions. The ground electrode was placed on the radial side of the humeral head. A heathy human

participant performed 3 bicep curls against gravity, with the elbow supported on their thigh. The Grapevine system manufactured by Ripple Neuro and the Micro-Star International (MSI) computer with a 9th generation intel core i7 processor were used to collect monopolar signals from each electrode at 30K Hz. The recorded data was imported and analyzed in Matlab (Mathworks). Recorded signals were differentiated between the pairs of electrodes with the same design. This differential signals were band-pass filtered between 10 and 500 Hz. The EMG signals from the circular electrodes were the least noisy with clearly separated EMG bursts (Fig. 10).

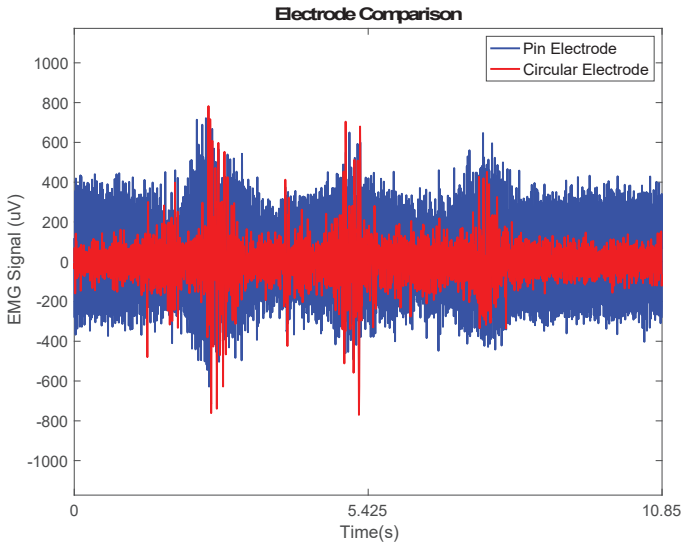

Figure 10: Representative recording of EMG through the array electrodes of different configurations. Differential EMG signal from a pair of pin electrodes without a separate electrode pad is shown in blue. Differential EMG signal from a pair of electrodes with circular pads is shown in red. Note the reduced amount of noise in the EMG from electrodes with the circular pads.

To quantify the quality of the EMG data, we calculated the signal to noise ratio (SNR) for each of the electrode types. This was done by calculating the standard deviation during an EMG burst corresponding to active muscle contractions and dividing it by the standard deviation of quiet periods where there is no muscle activity. The highest SNR was obtained from the circular electrodes (Fig. 11).

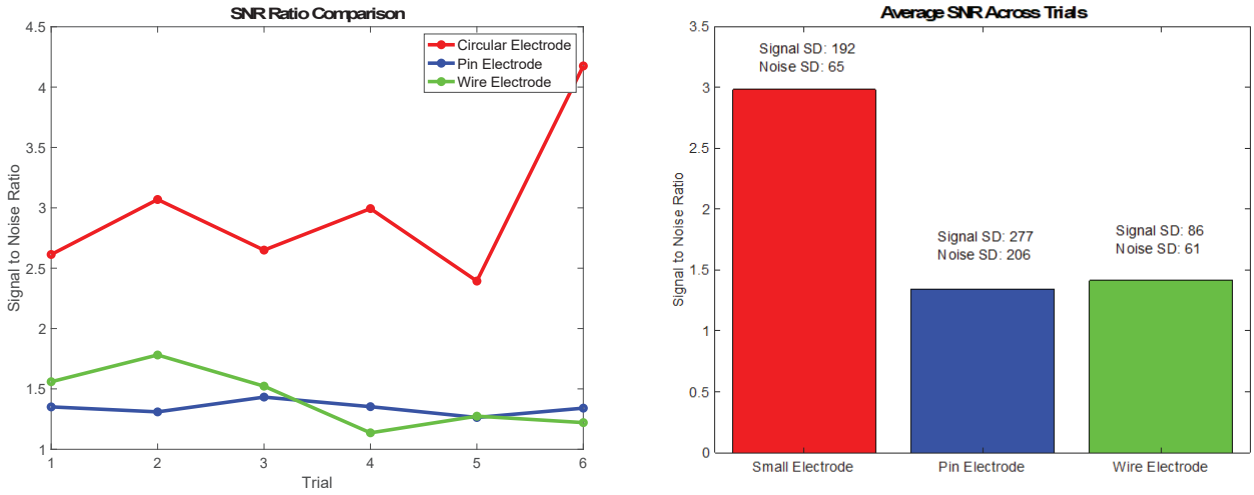

Figure 11. Signal to noise ratios for each electrode type. Left**:** The signal to noise ratio (SNR) during each movement). Right: SNR averaged across movements. The SNR for the EMG signals from the electrodes with circular pads (red) was much higher compared to SNR from the electrodes without pads (blue and green).

Building on top of our progress from the last reporting period, we used the optimal electrode type (small, smooth circular electrode) to build a high-density electrode array (Fig. 12). The band was 3D printed using thermoplastic polyurethane which gives it flexible properties while also being durable. It contains 145 circular holes to house electrodes that are spaced 10mm apart from each other, which falls into the optimal range for inter-electrode distance of a high-density EMG (hdEMG) device (Afsharipour 2019). Each electrode can be

unplugged and moved to any one of the 145 slots in the flexible band, allowing for extreme customizability of placement of our 64 recording electrodes.

Notable device properties:
Diameter: 4mm
Inter-electrode distance: 10mm
Average resistance across 64 electrodes: 24.75 Ohms
Maximum resistance: 34 Ohms
Minimum resistance: 19 Ohms
Array band material: Thermoplastic Polyurethane

Design and hardware integration for electrical stimulation through the custom-made array:

The stimulation array with larger electrode pads was manufactured for testing algorithms for shoulder muscle stimulation (Fig. 13, insert). The system will be controlled through the Grapevine output channels that will shape the output of the Digitimer stimulator system (Fig. 13).

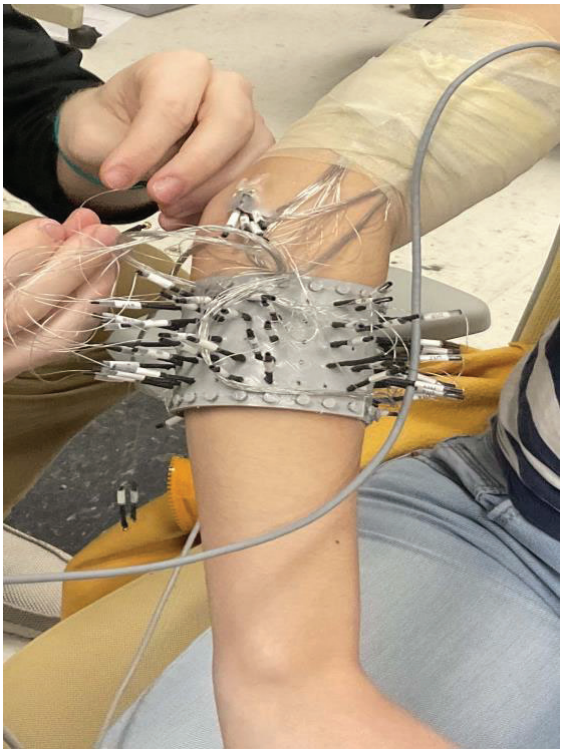

Figure 12: Flexible hdEMG array on the right forearm of the test subject.

Milestone #1: Submitted IP disclosure on the design of multichannel recording-stimulation electrode array

Done. The invention disclosure has been sent to the Corresponding Officer and the Contracting Specialist.

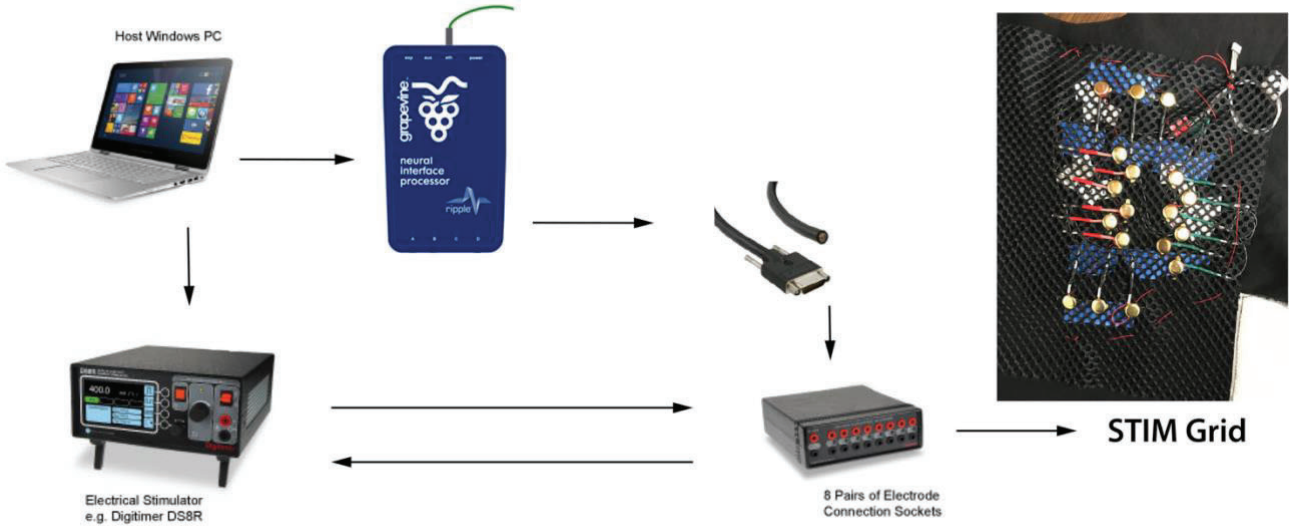

Figure 13: Hardware components of the high-density stimulation system.

Major Task 1.2: Obtaining normative data on high-density EMG

Subtask 1.2.1: HRPO regulatory review of hdEMG recording studies

We have obtained approval from the U.S. Army Combat Capabilities Development Command Armaments Center Human Research Protection Program to conduct human subject research under the protocol # 21-001 (PI - Dr. Yakovenko). The approval was obtained on the 25th of August 2021 (memo attached).

Milestone #2: Obtain HRPO approval for recording studies

Completed (please, see the approval letter in Attachments)

Subtask 1.2.2: Recruit healthy participants and conduct experiments with VR tasks recording hdEMG and motion capture

To test the quality of the data of the redesigned hdEMG array and the integration of the VR tasks with data collection pipelines, we conducted a test with one of the research team members. We placed the hdEMG array around the right forearm of the experimenter and asked her to perform various tasks that involved wrist and hand movements. These included simple, single degree of freedom (DOF) movements (hand open/close, wrist flexion/extension, wrist abduction/adduction, or wrist pronation/supination), and more complex compound movements moving a block over a barrier and back (virtual and real-time BBT improved under the Task 1.1.2). The simple movements were all performed with the elbow flexed at 90 degrees. Consistent pacing was achieved by having the subject follow videos of a model arm performing the desired movement on a screen. The real-world BBT task was performed using a 3D printed block. Two blocks of identical appearance but different weights were used to enable the study of the effect of object weight on the muscle activity patterns during object manipulation. Two force sensors were attached to the blocks to enable tracking of the timing of block pickup and drop and the estimation of grasping forces.

During the performance of these tasks, the Grapevine system (Ripple Neuro) was used to collect the data from the hdEMG array and the Trigno system (Delsys) was used to collect standard surface EMG data, accelerometer data, and force sensor data. We also recorded motion capture data using Leap imaging system during real-world tasks and Occulus hand tracking output during VR tasks. Additionally, timestamps obtained by each hardware data acquisition system from a custom server were also recorded for the development of data synchronization scripts.

To evaluate the quality of the hdEMG array design we differentiated, filtered, and plotted EMG signals during a wrist flexion trial from 2 pairs of electrodes that were located parallel to each other on the flexor digitorum muscle on the ventral side of the forearm (Fig. 15). We found that both signals were distinct (signal 1 showing a consistently higher amplitude than signal 2), representing activation of different motor units of the same muscle.

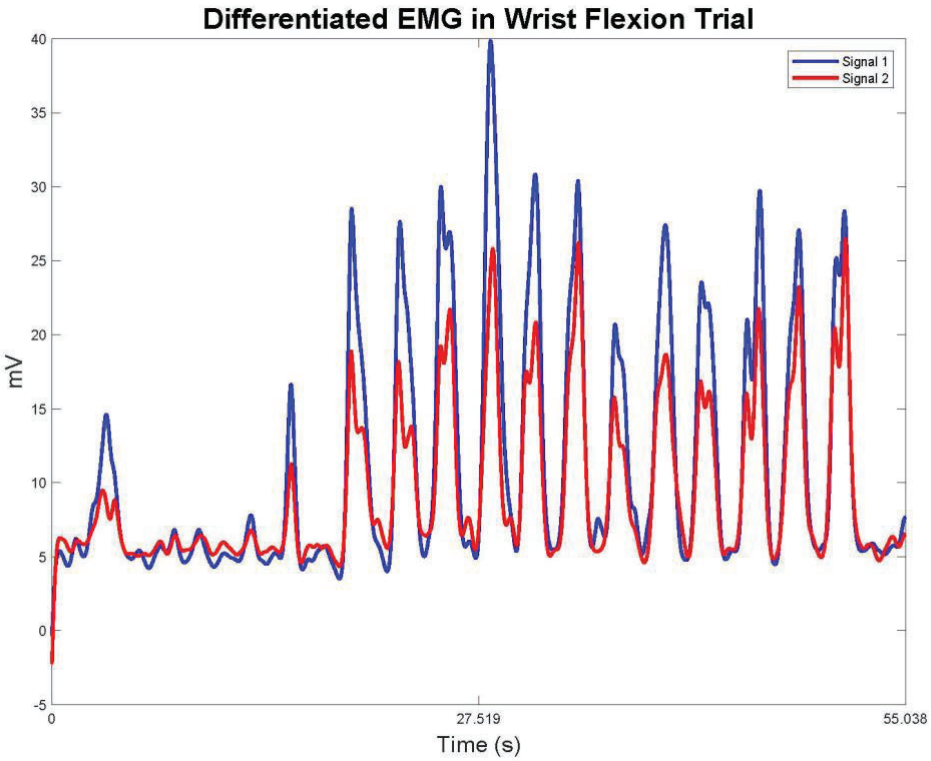

Figure 15: hdEMG signals from two pairs of electrodes during repeated movements. Upward deflections of both signals indicate increased muscle contraction. Both sets of electrodes were placed on forearm flexor muscle.

This is consistent with the published reports that muscles are not excited uniformly (Arvanitidis 2019). Furthermore, data in Figure 3 also shows that the envelope of activity detected by both pairs of electrodes overlaying the same muscle are in phase with each other, supporting the feasibility of identifying individual muscles from the overall hdEMG signals for use as control signals for electrical stimulation. The quality of the

data from the redesigned hdEMG array is also higher than the previous design, data from which was shown in the previous report.

Analysis of Leap motion capture data revealed a low and inconsistent rate of sampling of data during the performance of the real-world BBT. To mitigate this we will develop a head-mounting assembly to hold the Leap camera at an optimal angle.

Experimental design for normative data collection

Outline of the experimental design

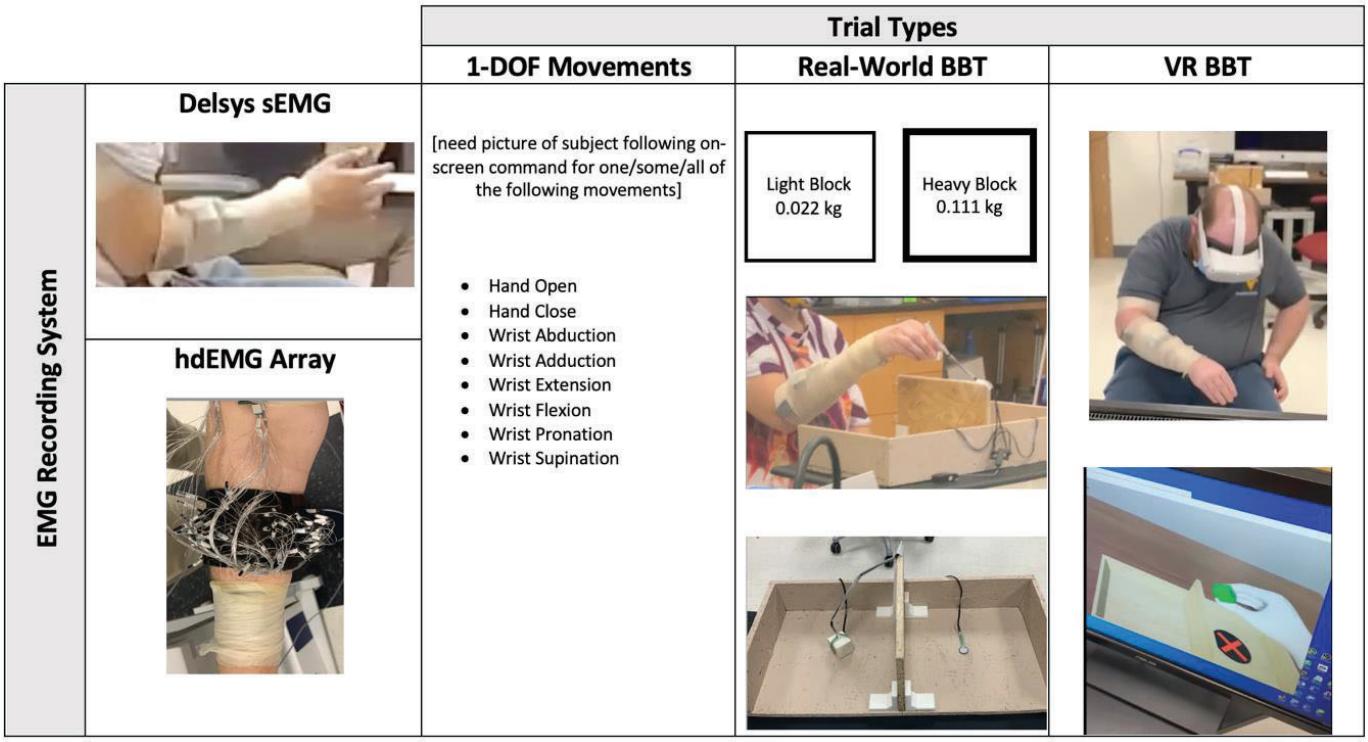

Subjects are asked to perform different movements (trial types) while EMG and motion are recorded using multiple systems. The first column shows two types of EMG systems (top: Delsys bipolar sensors and bottom: custom hdEMG array) that we are using to collect muscle activity. *Trial Types:* Single degree-of-freedom movements involved mimicking an on-screen avatar performing the movement with the subject's own hand. Real world box and block tests included both the use of a light-weight block (0.022 kg) and a heavy-weight block (0.111 kg). The subject are asked to move the block over the middle barrier 20 times while EMG and kinematics were recorded. FSR sensors were used to determine when the blocks were grasped, let go, picked up and placed back down. To illustrate the BBT with a block of 0 kg weight, VR was used. Subjects grasped the virtual green block, transported it over the barrier, and dropped it on the target 20 times. *EMG Recording System*: Delsys surface EMG sensors were used to collect the muscle activation of muscles in the thumb, forearm, upper arm, and shoulder. The custom hdEMG array contains 64 electrodes and is placed on the proximal end of the forearm to record high-density muscle activity.

The normative data using this experimental protocol was recorded from 4 participants by the end of the reporting period. An example of synchronized EMG and motion data during multiple repetitions of a single movement, wrist flexion and extension, is shown in Figure 16. The bursts of muscle contractions in a wrist flexor muscle coincide with the motion of the index finger with the hand toward flexion.

Subtask 1.2.3: Develop decoder to predict distal muscle activity from proximal hdEMG and disseminate results

Subtask 1.2.4: Develop an algorithm to predict the changes in proximal muscle activity due to motion of distal segments using MSD model

We collected data during different types of BBT, virtual, light-block, and heavy-block tasks, and several single- and multiple- degree of freedom movements. During reaching while holding the block in the BBT we observed that the muscle activity changed based on the weight of object being held and whether it was virtual

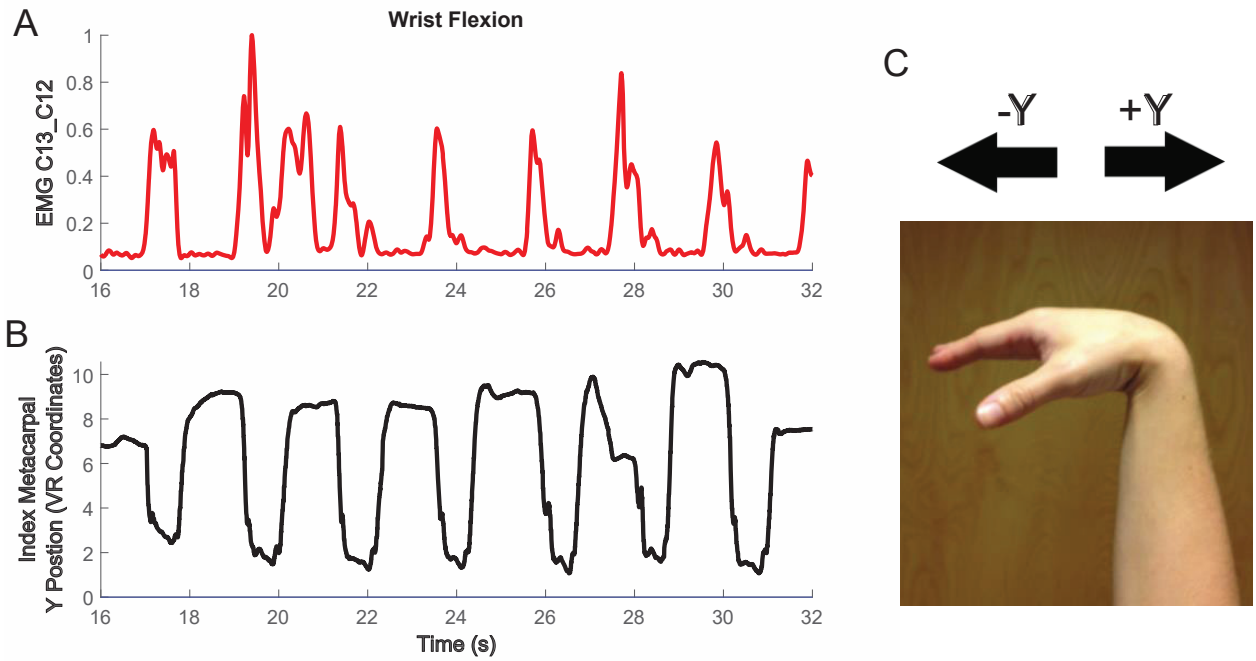

Figure 16. Example hdEMG Array and Kinematic Data During Wrist Flexion: *A)* The EMG is the filtered differential between electrode C13 and C12. We see obvious activations of the muscle that correspond to the flexion action. *B)* The representative kinematics are from the y-direction of the index finger. *C)* Demonstrates when the y position is decreasing (during flexion) and increasing (during extension).

or real object (Fig. 17). The temporal profiles of EMG signals from hand muscles differed across the tasks. Multiple muscles with agonistic and antagonistic actions around a given joint showed altered profiles, implying different levels of co-contraction associated with objects of different weight. These observations indicate that external forces caused by the object weight are compensated for by the nervous system through the co-contraction of muscles in order to increase the whole limb stiffness. This shows the feasibility of decoding proximal muscle activity from distal and vice versa.

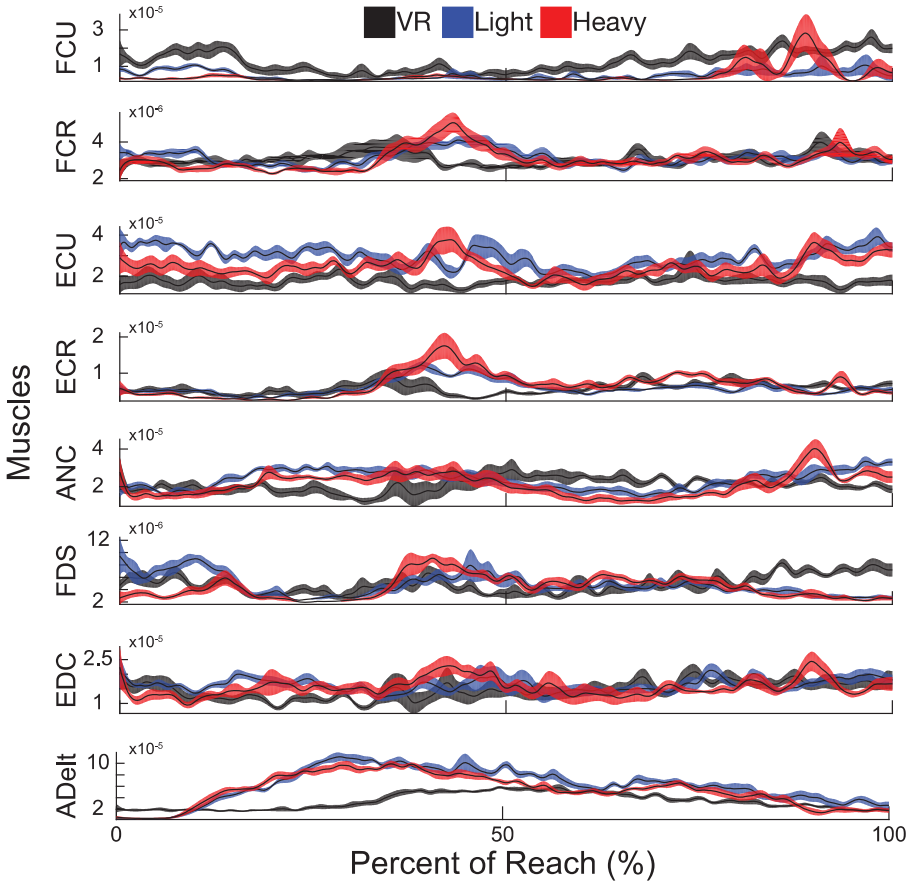

Figure 17. Delsys EMG during Box and Block Test. In this figure, the **black** EMG signals correspond to the EMG recorded during VR tasks (0.000 kg block), the **blue** EMG signals correspond to the real-world box and block test with the light (0.022 kg) block, the **red** EMG signals correspond to the real-world box and block test with the heavy (0.111 kg) block. The reach is normalized from 0 to 100% where 0 indicates the start of the reach toward the block (when the anterior deltoid begins to fire bringing the arm forward toward the block) on the left side of the box assembly and 100% is when the block is dropped on the right side of the box assembly.

Similar observations can be made from the hdEMG signals recorded with the custom array. We have achieved a very high signal to noise ratio of the hdEMG signals. The waveforms of hdEMG signals closely match the phase of the waveforms of the traditional Delsys EMG signals (Fig. 18). However, the shapes of the hdEMG waveforms differ, providing additional information about the recruitment of different muscles and muscle compartments.

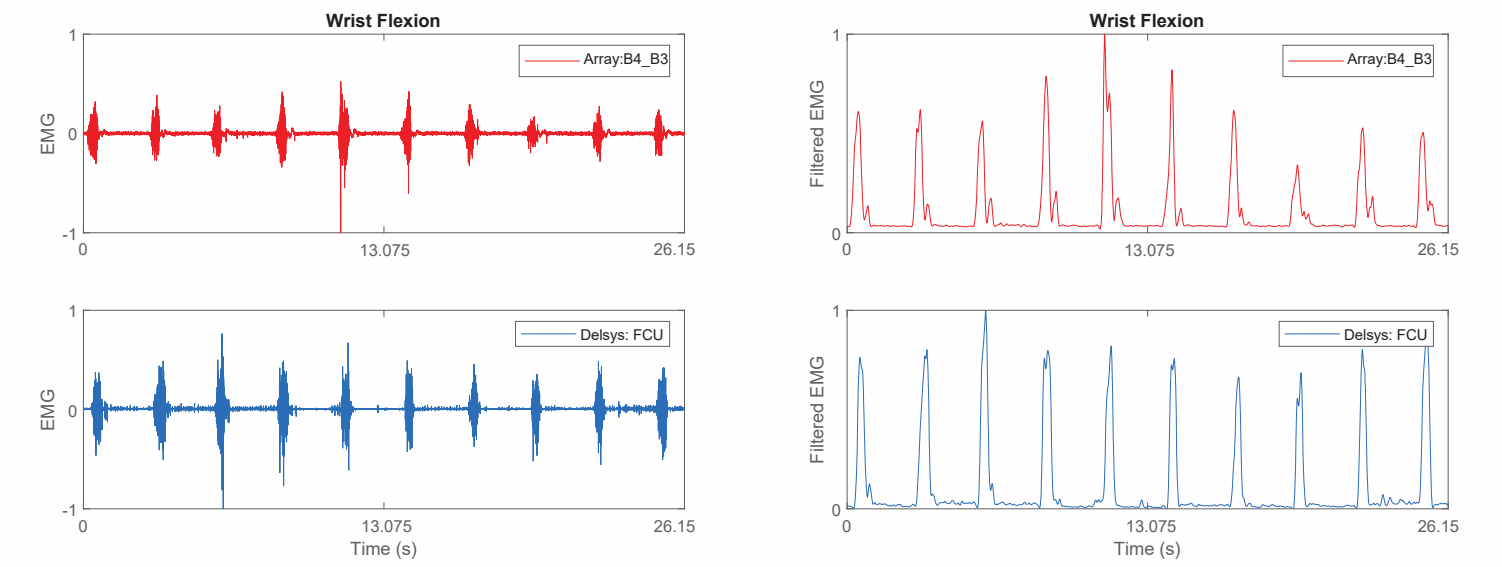

Figure 18. hdEMG Validation with Delsys sEMG. The red signals represent EMG during hdEMG Wrist Flexion trials (differential between electrodes B4 and B3), and the blue signals represent the EMG during the Delsys Wrist Flexion Trials (flexor carpi ulnaris). We see a distinct bursting pattern in each of the raw and filtered signals indicating that our custom built hdEMG array is capable of collecting EMG data similar to that of a "gold standard" commercially available EMG recording device.

Analysis of these data will be continued in the next reporting period for the decoding algorithm developments (see new timeline).

References

Ackland, D. C., Pak, P., Richardson, M., & Pandy, M. G. (2008). Moment arms of the muscles crossing the anatomical shoulder. *Journal of Anatomy*, *213*(4), 383–390. https://doi.org/10.1111/j.1469-7580.2008.00965.

Afsharipour, B, S Soedirdjo, and R Merletti. "Two-Dimensional Surface EMG: The Effects of Electrode Size, Interelectrode Distance and Image Truncation." *Biomedical Signal Processing and Control* 49 (2019): 298–307. https://doi.org/10.1016/j.bspc.2018.12.001.

Arvanitidis, Michail, Deborah Falla, and Eduardo Martinez-Valdes. "Can Visual Feedback on Upper Trapezius High-Density Surface Electromyography Increase Time to Task Failure of an Endurance Task?" *Journal of Electromyography and Kinesiology*, December 2019. https://doi.org/10.1016/j.jelekin.2019.102361.

Boots, M. T., Hardesty, R., Sobinov, A., Gritsenko, V., Collinger, J. L., Fisher, L. E., Gaunt, R., & Yakovenko, S. (2020). Functional and Structural Moment Arm Validation for Musculoskeletal Models: A Study of the Human Forearm and Hand. *BioRxiv*, 2020.05.29.124644. https://doi.org/10.1101/2020.05.29.124644

Folgado, J., Quental, C., Ambrósio, J., & Monteiro, J. (2013). Multibody System of the Upper Limb Including a Reverse Shoulder Prosthesis. *Journal of Biomechanical Engineering*, *135*. https://doi.org/10.1115/1.4025325

Graziano, M. S. A. (2016). Ethological Action Maps: A Paradigm Shift for the Motor Cortex. *Trends in Cognitive Sciences*, *20*(2), 121–132. https://doi.org/10.1016/j.tics.2015.10.008

Gritsenko, V., Krouchev, N. I., & Kalaska, J. F. (2007). Afferent Input, Efference Copy, Signal Noise, and Biases in Perception of Joint Angle During Active Versus Passive Elbow Movements. *Journal of Neurophysiology*, *98*(3), 1140–1154. https://doi.org/10.1152/jn.00162.2007

Just2Devs. Oculus Quest Hand Tracking. Youtube. https://www.youtube.com/playlist?list=PLbgD2Tk2QUnkYVdDN-EMSiinyKpWXRpIR

Kingma, D. P., & Ba, J. (2017). Adam: A Method for Stochastic Optimization. *ArXiv:1412.6980 [Cs]*. http://arxiv.org/abs/1412.6980

Mathiowetz, V., Volland, G., Kashman, N., Weber, K., 1985. Adult Norms for the Box and Block Test of Manual Dexterity. Am. J. Occup. Ther. 39, 386–391. https://doi.org/10.5014/ajot.39.6.386

Quental, C., Folgado, J., Ambrósio, J., & Monteiro, J. (2012). A multibody biomechanical model of the upper limb including the shoulder girdle. *Multibody System Dynamics*, *28*(1), 83–108. https://doi.org/10.1007/s11044-011-9297-0

Saul, K. R., Hu, X., Goehler, C. M., Vidt, M. E., Daly, M., Velisar, A., & Murray, W. M. (2015). Benchmarking of dynamic simulation predictions in two software platforms using an upper limb musculoskeletal model. *Computer Methods in Biomechanics and Biomedical Engineering*, *18*(13), 1445–1458. https://doi.org/10.1080/10255842.2014.916698

Smirnov, Y., Smirnov, D., Popov, A., & Yakovenko, S. (2020). Solving musculoskeletal biomechanics with machine learning. *BioRxiv*, 263962. https://doi.org/10.1101/2020.08.24.263962

Sobinov, A., Boots, M., Gritsenko, V., Fisher, L. E., Gaunt, R. A., & Yakovenko, S. (2019). Approximating complex musculoskeletal biomechanics using multidimensional autogenerating polynomials. *BioRxiv*, 759878. https://doi.org/10.1101/759878

Sobinov, A., Boots, M. T., Gritsenko, V., Fisher, L. E., Gaunt, R. A., & Yakovenko, S. (2020). Approximating complex musculoskeletal biomechanics using multidimensional autogenerating polynomials. *PLOS Computational Biology*, *16*(12), e1008350. https://doi.org/10.1371/journal.pcbi.1008350

Wagner, D. W., Stepanyan, V., Shippen, J. M., DeMers, M. S., Gibbons, R. S., Andrews, B. J., Creasey, G. H., & Beaupre, G. S. (2013). Consistency Among Musculoskeletal Models: Caveat Utilitor. *Annals of Biomedical Engineering*, *41*(8), 1787–1799. https://doi.org/10.1007/s10439-013-0843-1

What opportunities for training and professional development has the project provided?

Multiple training activities were available to the graduate students involved with the project. The PI Yakovenko and co-PI Gritsenko had weekly individual meetings, bi-weekly laboratory meetings, and bi-monthly project meeting with the students. Additionally, M. Yough, a PhD student of co-PI Gritsenko, has presented and published a conference paper stemming from his involvement with the project.

How were the results disseminated to communities of interest?

Nothing to Report.

What do you plan to do during the next reporting period to accomplish the goals?

We will continue collection of the normative data set. We will continue developing an EMG prediction algorithms using source localization techniques and principal component analysis. We will integrate musculoskeletal modeling into our data processing. We will also start testing different algorithms for the targeted controllable electrical stimulation of muscles.

4. Impact

What was the impact on the development of the principal discipline(s) of the project?

Results of our published conference paper have shown that both the solid and segmented forearm models perform well in simulating applied joint torques during naturalistic human movements, below 5% errors on average. The segmented model is preferred for applications where accuracy in the muscle moments driving pronation or supination is important. This performance is good enough for dynamic real-time simulations, for example, in biomimetic controllers. Both types of models can be scaled for individual body size with minimal reduction in the accuracy of dynamic simulations.

What was the impact on other disciplines?

Nothing to Report.

What was the impact on technology transfer?

We have developed a prototype of a new wearable device for high-definition recording and stimulation of muscles (see attached Technology Disclosure). This device can revolutionize the delivery of home-based therapies and performance assessment and training.

What was the impact on society beyond science and technology?

Nothing to Report.

5. Changes/Problems

Changes in approach and reasons for change

Nothing to Report.

Actual problems or delays and actions or plans to resolve them

Delay in the initiation of funding: The quarantine caused by COVID 19 epidemic has been partially lifted during the summer months and expected to be lifted completely during the fall semester. However, disruptions in administrative operations have been frequent. The negotiations by the WVU administration have not been resolved until early April, which was a disruption for the onset of our research activities.

Delay in the approval of IRB: We have continued revising of our IRB submission materials using feedback from DEVCOM. We have submitted several interactions of the documents with required revisions. This has delayed our human subject recruitment. To resolve this problem, we have continued to work with the HRPO and obtained approval after the end of reporting period.

Anticipated problems or delays and actions or plans to resolve them

Due to the aforementioned delays, the estimated time for completion of Subtasks 1.1.3, 1.2.3, and 1.2.4. and the time for achieving Milestones 3 and 4 has been changed. No additional delays are anticipated.

Changes that had a significant impact on expenditures

Nothing to Report.

Significant changes in use or care of human subjects, vertebrate animals, biohazards, and/or select agents

Nothing to Report.

Significant changes in use or care of human subjects

Nothing to Report.

6. Products

Publications, conference papers, and presentations

Yough, M. G., Hardesty, R. L., Yakovenko, S. and Gritsenko, V**.** (2021) A segmented forearm model of hand pronation-supination approximates joint moments for real time applications. *2021 10th International IEEE/EMBS Conference on Neural Engineering (NER),* pp. 751-754, doi: 10.1109/NER49283.2021.9441405. PMCID: PMC8243400.

Inventions, patent applications, and/or licenses

Gritsenko, V. Yakovenko, S., Yough, M., Korol, A. Design of Myoelectric Recording and Stimulation Array (MyoReSA) Office of Technology Transfer, West Virginia University Research Corporation. Copyright 2021.

7. Participants & Other Collaborating Organizations

Name:	Sergiy Yakovenko	Valeriya Gritsenko
Project Role:	PI	co-PI
Researcher Identifier:	https://orcid.org/0000-0002-5946-6409	https://orcid.org/0000-0002-6408-9433
Nearest person month worked:	2.2	2.0
Contribution to Project	No change	No change

8. Special Reporting Requirements

Updated Quad Chart is included.

9. Appendices

Closed-loop recording-stimulation system for accelerating recovery after musculoskeletal injury

Log Number DM190880

Funding Opportunity Number: W81XWH-19-DMRDP-CRMRP-RESTORE

PI: Yakovenko **Org:** West Virginia University **Award Amount:** $500,000.00

Study Aims

- Expand existing algorithms and devices for high-density electromyography with closed loop electrical stimulation (hdEMG-ES) to predict and intervene in the motion of distal segments using activity of proximal limb muscles.
- Control the motion of distal limb segments with stimulation based on the muscle activity of the proximal segments decoded with the MSD model.

Approach

We will validate and expand the MSD model of the arm to include shoulder degrees of freedom and integrate it with virtual reality (VR) and high-density electrode array. We will demonstrate non-volitional and fatigue-resistant control of forearm muscles with electrical stimulation through a high-density array in healthy participants performing tasks in VR. We will evaluate the system performance in participants with amputations and denervated muscles.

Accomplishment:

- Our team has demonstrated the feasibility of using the musculoskeletal model of the arm to identify synergistic muscle groups across multiple arm postures (Gritsenko et al., 2016). We have also demonstrated that a high-dimensional musculoskeletal model of the hand can be evaluated in real-time predicting motion from muscle activity (Yakovenko, DARPA HAPTIX quarterly reports 2014-2019, patent pending). We have identified the relationship between muscle activity and joint moments (Olesh et al. 2017) and found evidence for separate coordination of proximal and distal muscle groups (Hardesty et al. 2019).

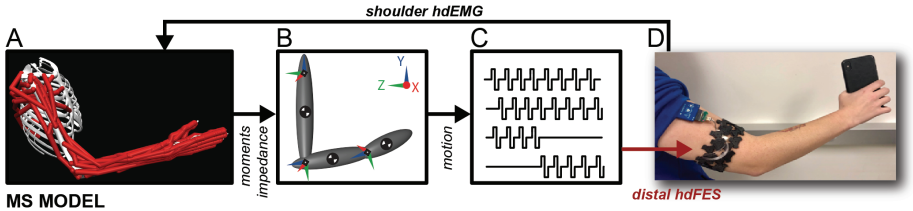

Timeline and Cost

Activities / CY	21	22	23
Develop hdEMG-ES system with VR tasks			
Determine the efficacy of the system to manipulate healthy muscle activity			
Test the efficacy of the system in amputees and those with arm denervation			
Estimated Budget ($K)	**$158**	**$169**	**$173**

Updated: 15 March 2022

Goals/Milestones

FY1 Goals – Expand on existing capabilities
- ✓ Building of hdEMG array and VR tasks
- ✓ Obtaining normative data and optimization of decoding algorithms
- ❑ Prediction of performance using big-data analysis methods

FY2 Goals – Add stimulation and test the system in controls
- ❑ Develop algorithms to stimulate muscles based on real-time predictions of muscle activity by MSD model
- ❑ Manipulate healthy intralimb coordination with hdEMG-ES

FY3 Goals – Quantify performance with full system and test the system in people with peripheral damage
- ❑ Demonstrate embedding of hdEMG-ES into the motor program for the healthy arm
- ❑ Test the efficacy of restoring intralimb coordination with hdEMG-ES after peripheral damage and in amputees

DEPARTMENT OF THE ARMY
U.S. ARMY COMBAT CAPABILITIES DEVELOPMENT COMMAND
ARMAMENTS CENTER
PICATINNY ARSENAL, NEW JERSEY 07806-5000

DEVCOM AC INSTITUTIONAL REVIEW BOARD (IRB)
INITIAL REVIEW APPROVAL LETTER

DOD Assurance # A20133
HHS Assurance # FWA00007405
New Project

To (CUI): Sergiy Yakovenko, Ph.D. **Date (U):** 25 August 2021

From (CUI): DEVCOM AC IRB
Eric N. Erickson, Jr., Chairman

DEVCOM AC IRB # 21-001

Project Title (CUI): Closed-loop Recording-stimulation System for Accelerating Recovery After Musculoskeletal Injury

Research Team Members (CUI): Valeriya Gritsenko, Ph.D., Brock A. Lindsey, M.D., & Sijin Wen, Ph.D.

Medical Monitor (CUI): Sebastian Brooke, M.D.

Sponsor (CUI): Congressionally Directed Medical Research Program

Performance Site (CUI):

West Virginia University, School of Medicine, Neural Engineering Laboratories (Erma Byrd Biomedical Research Facility (Rooms 151/150 & 144/145), 1 Medical Center Drive, Morgantown, WV 26506

Review Type (U): Full Board
Project Risk Level (U): Greater Than Minimal Risk
Current Risk Level (U): Greater Than Minimal Risk
Approval Date (U): 4 August 2021
Expiration Date (U): 3 August 2022

Documents Reviewed and Approved (CUI):

- Adverse Device Effect – FDA
- Info Sheet -Sig Risk_Non Med Dev_FDA Jan 2016
- Information Sheet-FAQs Medical Devices FDA Jan 2006
- Array manufacturing 20210608 v2
- Array manufacturing 20210610 v3
- Memorandum 20210610 v1
- Array manufacturing 20210702 v5
- IRB pre-meeting answers
- Leap_Motion_Controller_Datasheet
- Prochazka et al. - 1992 - Attenuation of pathological tremors by FES
- Form 109 CCDC-AC Investigator Disclosure Form VG
- Gritsenko BRI
- GritsenkoCV
- VG citiCompletionReport2090397 good clincial practice
- Hana CITI Biomedical Research Investigators

- Hanna – CV
- Hanna GCP
- Brock BRI
- Brock GCP
- Form 109 CCDC-AC Investigator Disclosure Form BL
- Lindsey_Brock_CV
- Form 109 CCDC-AC Investigator Disclosure Form SW
- Wen BRI
- Wen GCP
- Wen_Sijin_CV
- Form 109 CCDC-AC Investigator Disclosure Form SY
- Yakovenko – CV
- Yakovenko CITI Biomedical Research Investigators 2023-01-02
- Yakovenko CITI GCP
- Form 201-A CCDC AC IRB IR Sub Checklist (v1) 20210305 SIGNED
- SOW (v1) 20210105
- ICF OMR RESTORE (v1) 20210311
- Recruitment flyers (v1) 20210305
- Screening Checklist 20210305_v1
- Study protocol (v1) 20210311
- Approval Letter WVU IRB 1912827265
- ApprovalLetter WVU IRB 1311129283
- ApprovalLetter WVU IRB 1906597769
- Children Assent Form WVU IRB 1912827265
- ICF MMR WVU IRB 1906597769
- ICF OMR WVU IRB 1311129283
- IFC OMR WVU IRB 1912827265
- Protocol WVU IRB 1311129283
- Protocol WVU IRB 1906597769
- Protocol WVU IRB 1912827265
- 21-001 ICF_OMR_IRB Edits_20210716
- 21-001 Proj App Form_(v2) 20210405
- 21-001 Recruitment_flyers_20210716_IRB Edits
- 21-001 Screening_Checklist_20210716_IRB Edits
- 21-001 Study protocol 20210716_IRB Edits
- Array manufacturing 20210610 v3
- Device_DS7A Specifications
- Device_Tringo Specifications
- DoD_ Program Information Paper
- DoD_Funding Notification Letter DOD RESTORE
- DoD_Peer Review Summary Statement
- IAIR 2020-006 West Virginia University 20201016
- Risk Memorandum 20210610 v1
- STTR - Gritsenko - Motion From Muscle Activity
- 20-001 Array Manufacturing_20210816_clean
- 20-001 Array Manufacturing_20210816_tracked
- 21-001 ICF_OMR_IRB Edits_20210816_clean
- 21-001 ICF_OMR_IRB Edits_20210816_tracked

- 21-001 Recruitment_flyers_20210816_clean
- 21-001 Recruitment_flyers_20210816_tracked
- 21-001 Screening_Checklist_20210816_clean
- 21-001 Screening_Checklist_20210816_tracked
- 21-001 Study protocol 20210816_clean
- 21-001 Study protocol 20210816_tracked
- 21-001 ICF_OMR_IRB Edits_20210716_WVU_v2
- 21-001 Study protocol 20210716_IRB Edits_v2
- Adverse Event Log Template 20210628 v1
- Brooke CITI 202501
- Brooke COI Med Monitor Form
- Brooke CV June 2021
- Brooke Medical Monitor Form_21-001
- EWave_Zynex_Manual_Rev_05
- Grapevine_Ripple_User_Manual_short
- Impulse_PhaseSpace_USERS-MANUAL-646538
- Prepaid card system WVU
- Prochazka et al. - 1992 - Attenuation of pathological tremors by FES
- VIVE Specs & User Guide - Developer Resources
- Gritsenko CITI Exp 202304
- Gritsenko CITI Exp 20210823
- Gritsenko COI
- GritsenkoCV
- Brock CITI Exp 20211012
- Brock COI
- Brock GCP CITI Exp 202107
- Lindsey_Brock_CV
- Wen BRI CITI Exp 202403
- Wen COI
- Wen GCP CITI Exp 202108
- Wen_Sijin_CV
- Yakovenko – CV
- Yakovenko CITI BRI Exp 202301
- Yakovenko CITI GCP Exp 202401
- Yakovenko COI
- 21-001 IR Sub Checklist (v1) 20210305 SIGNED (1)
- 21-001 Project Application Form_Extra Staff (v2) 20210405 (1)
- 21-001 ICF_Neuromuscular Deficit_IRB Edits
- 21-001 ICF_OMR_IRB Edits
- 21-001 ICF_OMR_v1_20210405
- 21-001 ICF_OMR_v1_20210405
- 21-001 IR Sub Checklist (v1) 20210305
- 21-001 Proj App Form_(v2) 20210405
- 21-001 Recruitment_flyers_IRB Edits
- 21-001 Recruitment_flyers_v1_20210405
- 21-001 Screening_Checklist_IRB Edits
- 21-001 Screening_Checklist_v2_ 20210405 (1)
- 21-001 Study protocol (v2) 20210405 (2)

- 21-001 Study protocol (v2) 20210405 (2)
- 21-001 Study protocol 20210405_IRB Edits
- 21-001 Supporting_documentation
- DoD Program Information Paper
- Funding Notification Letter DOD RESTORE
- Peer Review Summary Statement
- Specifications_recording_devices
- Specifications_stimulating_devices
- STTR - Gritsenko - Motion From Muscle Activity

1. (U) This new project submission was reviewed and approved via full board review by the DEVCOM AC IRB on 4 August 2021. The DEVCOM AC Human Research Protection Official (HRPO) Review was conducted and approved on 25 August 2021. Scientific Review was considered by the IRB during their review. The project was found to comply with applicable Federal, DOD, U.S. Army, and DEVCOM AC Human Research Protections Program (HRPP) requirements.

2. (U) This project was approved for the enrollment of up to 108 subjects. The project is Active – Open to Enrollment.

3. (U) The DEVCOM AC IRB served in the capacity of a Privacy Board for the HIPAA Authorization. The DEVCOM AC IRB members approved a partial waiver of the Authorization requirements of the Privacy Rule as you are requesting access to PHI as necessary means to identify a subpopulation within the study (i.e., for 8 subjects of the 108 approved for the research). The Board members discussed that it was not necessary to waive the Authorization requirement for the entire research study, but to partially waive the Authorization requirement to permit a covered entity to disclose PHI to the PI for the purposes of contacting and recruiting eight (8) individuals into the study.

4. (U) The following are reporting requirements and responsibilities of the Principal Investigator (PI) to the DEVCOM AC HRPP. Failure to comply could result in suspension of funding.

a. (U) The PI is responsible for fulfilling regulatory reporting requirements to the DEVCOM AC IRB as outlined in DEVCOM AC Standard Operating Procedures.

b. (U) Significant changes such as major non-administrative changes; change in PI within the same institution must be are acknowledged by the HRPP after IRB approval. Substantive modifications to the research protocol and any modifications that could potentially increase risk to subjects must be submitted to the HRPP for acceptance prior to implementation. The DEVCOM AC HRPP/HRPO defines substantive modification as the addition of an external PI, change or addition of an institution, elimination or alteration of the consent process, change to the study population that has regulatory implications (e.g. adding children, adding active duty population, etc.), significant change in study design (i.e. would prompt additional scientific review) or a change that could potentially increase risks to subjects or the addition of research that requires approval from the Office of the Under Secretary of Defense for Research and Engineering (OUSD(R&E)) or (USD(R&E)) or approval from the Head of the Office of the Secretary of Defense (OSD) or DOD Component as delegated by (OUSD(R&E)) (e.g., classified research, research with prisoners).

c. (U) All unanticipated problems involving risk to subjects or others must be promptly reported by telephone (973-724-4958), by email (usarmy.pica.ccdc-ac.mbx.hrpo@mail.mil), to the DEVCOM AC HRPP. A complete written report will follow the initial notification. In addition to the methods above, the complete report can also be sent to the U.S. Army Combat Capabilities Development Command,

Armaments Center, ATTN: DEVCOM AC HRPP, 4th Street, Bldg. 62N, Picatinny Arsenal, New Jersey 07806-5000.

d. (U) Suspensions, clinical holds (voluntary or involuntary), or terminations of this research by the IRB, the institution, the sponsor, or regulatory agencies will be promptly.

e. (U) The final study report submitted to the DEVCOM AC IRB, including a copy of any acknowledgement documentation and any supporting documents, must be submitted to the HRPP as soon as all documents become available.

f. (U) The knowledge of any pending compliance inspection/visit by the HHS - Office for Human Research Protections, or other government agency concerning this research project; the issuance of Inspection Reports, warning letters or actions taken by any regulatory agency including legal or medical actions; and any instances of serious or continuing noncompliance

5. (U) This project was approved with (1) written informed consent document. Where obtaining informed consent/permission/assent is required as a condition of approval, be sure to assess subject capacity, and continue to monitor the subject's willingness to participate throughout the duration of the study. Use current DEVCOM AC IRB stamped forms in the consent process. Each subject must receive a copy of his/her signed consent/permission/assent document.

6. (U) Any modifications, (e.g., changes in the principal investigator, inclusion/exclusion criteria, number of subjects to be enrolled, study sites, or procedures) must be submitted as a written amendment for DEVCOM AC IRB review and approval prior to implementation. All reportable events including those that may affect the safety or rights of the subject, the integrity of the data and unanticipated problems involving risks to subjects or others must be reported promptly to the DEVCOM AC IRB.

7. (U) You are reminded that you must apply for, continuing review, and be granted continued approval for this study before 3 August 2022, to conduct your study in an uninterrupted manner. If you do not receive approval before this date, you must stop all research involving human subjects, their tissue and their data until such time as IRB approval is granted. A continuing review application must be submitted to the DEVCOM AC IRB no later than 3 July 2022, to ensure approval on or before 3 August 2022.

8. (U) This IRB approval is not a start letter and your center or institution that covers the DOD Assurance that you conduct your research under may have additional requirements that must be met. Please contact your Human Protections Director for local requirements that must be met prior to the start of your study.

9. (U) The DEVCOM AC HRPP POC for this study is Jason Symak at 973-724-3861 or jason.j.symak.civ@mail.mil.

Please include your project title and DEVCOM AC IRB # in all correspondence with this office.

A segmented forearm model of hand pronation-supination approximates joint moments for real time applications*

Matthew G. Yough, Russell L. Hardesty, Sergiy Yakovenko, and Valeriya Gritsenko

Abstract— **Musculoskeletal modeling is a new computational tool to reverse engineer human control systems, which require efficient algorithms running in real-time. Human hand pronation-supination movement is accomplished by movement of the radius and ulna bones relative to each other via the complex proximal and distal radioulnar joints, each with multiple degrees of freedom (DOFs). Here, we report two simplified models of this complex kinematic transformation implemented as a part of a 20 DOF model of the hand and forearm. The pronation/supination DOF was implemented as a single rotation joint either within the forearm segment or separating proximal and distal parts of the forearm segment. Torques produced by the inverse dynamic simulations with anatomical architecture of the forearm (OpenSim model) were used as the "gold standard" in the comparison of two simple models. Joint placement was iteratively optimized to achieve the closest representation of torques during realistic hand movements. The model with a split forearm segment performed better than the model with a solid forearm segment in simulating pronation/supination torques. We conclude that simplifying pronation/supination DOF as a single-axis rotation between arm segments is a viable strategy to reduce the complexity of multi-DOF dynamic simulations.**

I. Introduction

Musculoskeletal models are useful tools in bottom-up descriptions of body mechanics for theoretical and engineering applications. A detailed biomechanical dynamic model of the human upper extremity was developed in OpenSim by Saul et al. [1], [2]. This and similar arm models have been used in human-machine interfaces [3]–[6] and biomimetic control systems for prosthetics [7]–[9]. This promising application embeds musculoskeletal models in closed-loop control systems, which can be implemented in Matlab (MathWorks, Inc.) with OpenSim application programming interface. Such hybrid control systems have been successfully implemented using both forward and inverse dynamic simulations [10]. However, each additional mechanical degree of freedom (DOF) in these models requires additional differential equations for simulating segmental dynamics. Solving these equations in real-time for closed-loop control of complex human anatomy remains challenging [11], [12]. For example, the human hand and forearm are comprised of 17 complex joints with at least 30 DOFs. Therefore, reducing the number of simulated DOFs is a practical means to simplify the implementation of biomimetic algorithms in closed-loop control systems. For example, pronation/supination of the wrist results from the rotation of both the ulna and radius along their respective longitudinal axes (2 DOFs). However, the resulting motion of the hand can be described as a single DOF about the forearm. Thus, it is possible to simulate the pronation/supination of the hand as a single-DOF revolute joint, reducing the number of differential equations that must be solved in real-time. The questions addressed in this study are how to define this hand/forearm simplification relative to the underlying anatomy and whether to model the forearm as one segment, as implemented in [13], or as two segments. These simplifications, however, still need to reflect accurately the joint moments produced by muscles. Body anatomy is embedded in the neural control signals [14], [15] and any mismatch between the intended biological and simulated forces will degrade the performance of a biomimetic system. Moreover, inverse simulations aimed at estimating muscle activity patterns and neural control signals from joint moments would be similarly affected by inaccuracies caused by model simplifications. In this study, we quantified the errors in predicting joint moments with inverse simulations that are caused by the simplification of pronation/supination as a single-DOF joint and developed a solution which reduced these errors.

II. Methodology

A. OpenSim Model

We used a published model of an arm with 3 joints and 7 DOFs that was implemented in OpenSim 4.1[1], [2]. The pronation/supination DOF was defined as a rotation of the radius about the ulna and the joint torque was measured about an axis parallel to the ulna segment (Fig. 1). To represent the variability of hand forces during naturalistic human movements we extended the model to articulate the hand with 16 DOFs, bringing the total number of DOFs to 20 as reported in [16]. The kinematic chain of hand segments was organized

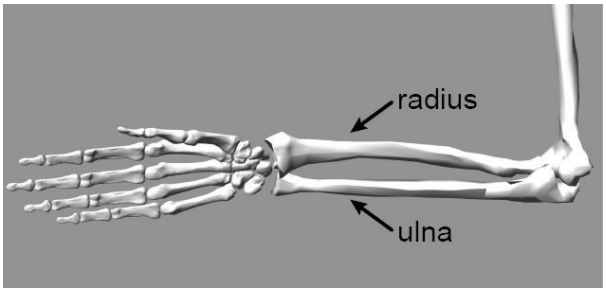

Figure 1. OpenSim model illustrating the anatomy of the forearm and hand segments. The pronation/supination is accomplished by radius rotating around the ulna.

*Research supported by National Institute of General Medical Sciences and the National Institute of Child Health and Human Development.

M. G. Y. Author is with West Virginia University, Morgantown, WV 26506 USA (phone: 304-293-7976; fax: 304-293-7105; e-mail: mgy0003@mix.wvu.edu).

R. L. H. Author was with West Virginia University. He is now with the National Center for Adaptive Neurotechnologies, Stratton VA Medical Center, Albany, NY 12208 USA (e-mail: hardesty@neurotechcenter.org).

S. Y. Author is with West Virginia University, Morgantown, WV 26506 USA (e-mail: seyakovenko@mix.wvu.edu).

V. G. Author is with West Virginia University, Morgantown, WV 26506 USA (e-mail: vgritsenko@mix.wvu.edu).

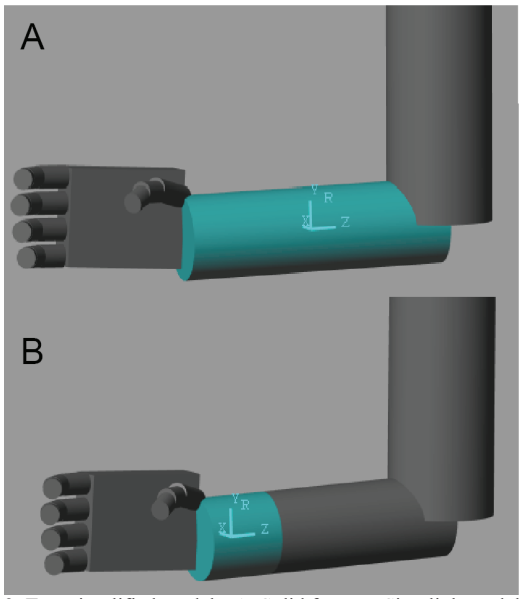

Figure 2. Two simplified models. A. Solid forearm Simulink model. Axes show a local coordinate system of the forearm segment. B. Segmented forearm Simulink model. Axes show a local coordinate system of the distal forearm segment.

from proximal segment (parent) to distal segment (child), i.e., from metacarpals, proximal phalanges, middle phalanges, and to distal phalanges. The segments of the hand that include carpal and metacarpal bones were modeled as a single rigid body with the inertia matrix of a rectangular prism (Fig. 2). The segments of digits were modeled as cylinders. The center of mass was placed in the center of each segment. The dimensions and inertial parameters of segments were based on published anthropometric data for humans of varied body sizes from 5% to 50% (average) to 95% of normal range [17], [18].

The joints were modeled as ideal joints with zero stiffness and viscosity. The carpometacarpal joint was modeled with two DOFs (thumb flexion/extension and abduction/adduction), and each of the rest of the 14 finger joints was modelled as hinge joints with one DOF (phalangeal flexion/extension). Local coordinate systems of bodies and joints were selected so that flexion was positive in all hand DOFs, and thumb abduction was positive.

B. Simulink Model

We developed two equivalent upper extremity models in Simulink (MathWorks, Inc). Both Simulink models matched the OpenSim model in all inertial and morphometric parameters with the exception of the forearm segment and pronation/supination joint. In the first Simulink model, referred to as solid forearm model, the forearm segment was a single cylinder with inertial parameters closely matched to the geometric sum of radius and ulna bodies of the OpenSim model (Fig. 2A). The center of mass was placed in the center of the forearm segment. The pronation/supination torque was measured between the humerus segment fixed in the world reference frame and the forearm segment about the Z axis in Fig. 2A. In the second Simulink model, referred to as segmented forearm model, the forearm segment from the first model was split into two cylinders (Fig. 2B). The pronation/supination torque was measured between the proximal and distal compartments of the forearm segment about the Z axis in Fig. 2B. The center of mass was placed in the center of each segment.

C. Inverse Dynamics

Movements of the hand were simulated to mimic characteristic point-to-point human movement with a bell-shaped velocity profile [19]. A total of 65 movements were simulated representing 13 hand movements each repeated at 0º, 45º, or 90º elbow flexion or with concurrent flexion or extension of elbow through 0º - 130º range. The simulated hand movements were as follows: 1) wrist pronation, 2) wrist supination, 3) wrist flexion and adduction, 4) wrist extension and abduction, 5) closing the hand, 6) opening the hand, 7) closing the hand and wrist pronation, 8) opening the hand and wrist pronation, 9) closing the hand and wrist supination, 10) opening the hand and wrist supination, 11) while in supination, closing the hand and flexing the wrist, 12) while in pronation, opening the hand and extending the wrist, and 13) hand opening while the thumb is flexing. The angular kinematics of each moving DOF for a given movement was approximated as a symmetrical sigmoidal trajectory in time lasting 0.5 seconds (Fig 3A). The trajectory was scaled in amplitude to the appropriate range for each movement. In most movements, the starting posture for all DOFs was a neutral, i.e., the half-way angle between the maximal and minimal range of the corresponding DOF. The stopping angle was at 45% of maximal or minimal range derived from published ergonomic data [18]. The polynomial coefficients of the scaled trajectory were then differentiated to calculate angular velocity and differentiated again to calculate angular acceleration. The angular position of the non-moving DOFs were set to the required posture (neutral posture, elbow at 0º, 45º, or 90º flexion angle, or full pronation or supination) with zero velocity and acceleration.

We computed applied joint torques for all models using inverse dynamics driven by angular kinematics of each of the 65 movements. Simulations with the OpenSim model were run using the inverse dynamics tool of OpenSim MATLAB API. The torques were low-pass filtered at 6 Hz. Simulations with the Simulink models were ran using 4th order Runge-Kutta solver with a fixed 1 ms timestep. Simulations with models of different body sizes were ran to test the generality of our conclusions for the analysis of kinematic data from individuals of different sizes. The OpenSim and Simulink joint torques were compared by calculating root-mean-squared-error (RMSE) for each DOF for all movements. The RMSE values were normalized to the torque range of the OpenSim model per DOF per movement.

III. Results

Applied torques calculated with inverse dynamics were on similar scale across all models for all movements. The mean RMSEs were below 5% of peak-to-peak torque for most DOFs across all movements. This shows that the inverse dynamic calculations in OpenSim API and Simulink are similar despite any differences in their respective algorithms. The differences between models were, as expected, primarily in pronation-supination torques.

The applied torque about the pronation/supination DOF of the segmented model was the most similar to that produced by anatomical joints simulated in OpenSim (Fig. 3B). The

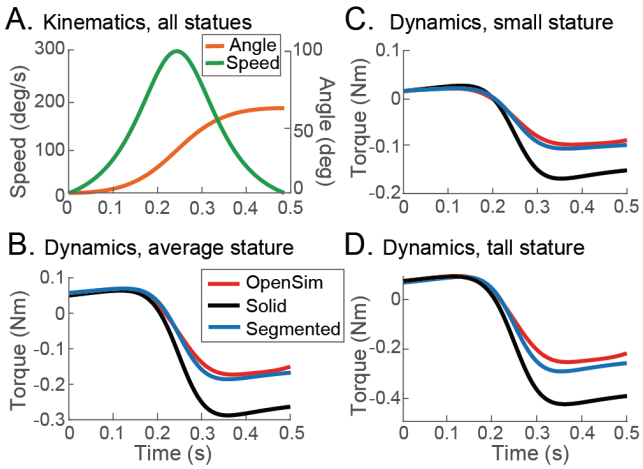

Figure 3. Trajectories for pronation/supination DOF from inverse dynamic simulation of a movement 1) as described in methods with elbow at 90º. A. Angular kinematics that served as input into the simulation (acceleration is not shown). B. Applied torque, the output of the simulations with the OpenSim and two Simulink models (solid and segmented) scaled to the average body size (50th percentile of normal range). C & D. Same as B for models scaled to the small and tall body size respectively (5th and 95th percentiles respectively).

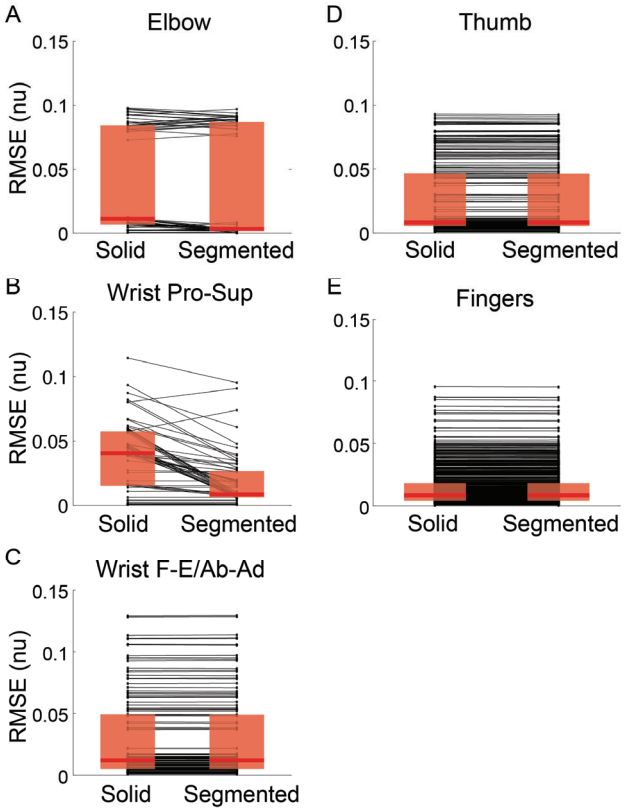

Figure 4. Torque errors between solid and segmented Simulink models and OpenSim model. A-E: Errors for torques about individual joints. Black lines connect RMSE values for corresponding movements, red lines are averages with shaded rectangles indicating interquartile range. Pro-Sup indicated pronation and supination; F-E indicated flexion and extension; Ab-Ad indicates abduction and adduction; nu indicated normalized units.

forearm architecture had a generally small effect on the torque accuracy across all movement and DOFs (Fig. 4). As expected, the largest effects of forearm architecture on torque accuracy across all movements was at pronation/supination and elbow DOFs (Fig. 4A & B). These errors were driven by the differences in offset, as illustrated in Fig. 3B, or in profiles that affected the peak values of applied torques and sometimes both. This shows that simulations with solid forearm models could be wrong by up to 15% in estimating the amplitude of postural and propulsion-related muscle forces.

Torque profiles obtained for the models of short and tall human body sizes varied in scale, but not profiles (Fig. 3C & D). The errors between the corresponding OpenSim and segmented models generally increased with body size but remained mostly below 15% of peak-to-peak torque (Fig. 5). The scaling of errors with body size was the most prominent in torques about the wrist and finger joints in movements with concurrent elbow motion. This is likely due to the cumulative effect of numerical errors that propagate from proximal to distal joints and have a larger effect on smaller distal torques.

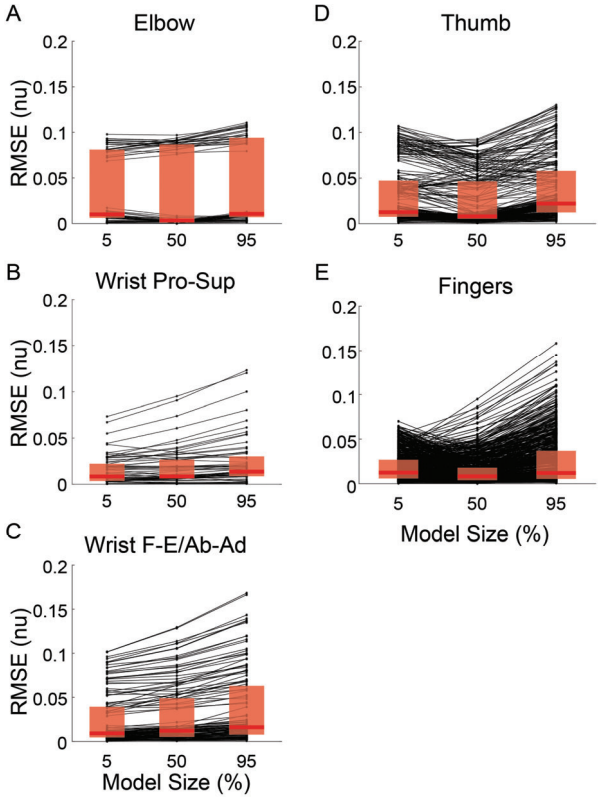

Figure 5. Torque errors between segmented Simulink model and the corresponding OpenSim model scaled to short (5%), average (50%), and tall (95%) body sizes. Formatting as in Figure 4.

IV. Discussion and Conclusion

Despite known difficulties in obtaining consistent solutions across platforms [20], we have achieved very close inverse simulation results between OpenSim and Simulink models. Even the model with extremely simplified pronation/supination joint placed in the cylindrical solid forearm segment produced joint torques that were closely matched to those of a model with separate ulna segment rotating about the radius segment through complex joints (Fig. 4). These errors were mostly below 10% of peak-to-peak torques across all simulated joints and movements, with

pronation/supination being the most adversely affected DOF. Our results have shown that when the accuracy of muscle moments about the wrist is not crucial, a simplified pronation/supination joint with a single DOF placed in the elbow can provide reasonable approximations for biomedical applications.

The segmented forearm model in Simulink performs with high precision across all tested movements. The errors were within the range of perceptual errors in joint position measured in psychometric human studies [21]. The uneven split into proximal and distal cylindrical segments closely matches the moments of inertia of the radius segment rotating about the ulna segment and results in the smallest errors between OpenSim and Simulink models (Fig. 4). This model still simulates pronation/supination as a single DOF about an axis parallel to both compartments of the forearm segment, providing the benefit of a simplified dynamic simulation. This result has direct implications for neuroprostheses. The myoelectric control of actuated hand prostheses in transradial amputees may be improved by embedding the segmented model into the decoding algorithm. Such a model could be more accurate in predicting the intended motion from contractions of residual muscles involved in pronation and supination, such as pronator teres, supinator, biceps, and extensor and flexor carpi radialis and ulnaris muscles.

The accuracy of simulations with movement of the elbow were sensitive to body size. In these movements, the errors scaled with model size by less than 1% on average, the worst single-movement simulation showing 15% errors about finger joints (Fig. 5E). This cannot be explained by the change in body inertia because RMSE values were normalized to the peak-to-peak torque, which scaled with body size. This normalization did not remove the trend, indicating that the errors in numerical methods for solving differential equations may be the culprit. Our results show that the cumulative effect of these numerical errors in simulations with movement of proximal joints is the largest at distal joints.

In conclusion, both the solid and segmented forearm models performed well in simulating applied joint torques during naturalistic human movements, below 5% errors on average. The segmented model is preferred for applications where accuracy in the muscle moments driving pronation or supination is important. This performance is good enough for dynamic real-time simulations, for example, in biomimetic controllers. Both types of models can be scaled for individual body size with minimal reduction in the accuracy of dynamic simulations.

REFERENCES

[1] K. R. Saul *et al.*, "Benchmarking of dynamic simulation predictions in two software platforms using an upper limb musculoskeletal model," *Comput. Methods Biomech. Biomed. Engin.*, vol. 18, no. 13, pp. 1445–1458, Oct. 2015, doi: 10.1080/10255842.2014.916698.

[2] K. R. S. Holzbaur, W. M. Murray, and S. L. Delp, "A Model of the Upper Extremity for Simulating Musculoskeletal Surgery and Analyzing Neuromuscular Control," *Ann. Biomed. Eng.*, vol. 33, no. 6, pp. 829–840, Jun. 2005, doi: 10.1007/s10439-005-3320-7.

[3] T. Kapelner, M. Sartori, F. Negro, and D. Farina, "Neuro-Musculoskeletal Mapping for Man-Machine Interfacing," *Sci. Rep.*, vol. 10, no. 1, p. 5834, Dec. 2020, doi: 10.1038/s41598-020-62773-7.

[4] A. J. Nelson, P. T. Hall, K. R. Saul, and D. L. Crouch, "Effect of Mechanically Passive, Wearable Shoulder Exoskeletons on Muscle Output During Dynamic Upper Extremity Movements: A Computational Simulation Study," *J. Appl. Biomech.*, vol. 36, no. 2, pp. 59–67, Apr. 2020, doi: 10.1123/jab.2018-0369.

[5] L. Peternel, C. Fang, N. Tsagarakis, and A. Ajoudani, "A selective muscle fatigue management approach to ergonomic human-robot co-manipulation," *Robot. Comput.-Integr. Manuf.*, vol. 58, pp. 69–79, Aug. 2019, doi: 10.1016/j.rcim.2019.01.013.

[6] R. J. Varghese, B. P. L. Lo, and G.-Z. Yang, "Design and Prototyping of a Bio-Inspired Kinematic Sensing Suit for the Shoulder Joint: Precursor to a Multi-DoF Shoulder Exosuit," *IEEE Robot. Autom. Lett.*, vol. 5, no. 2, pp. 540–547, Apr. 2020, doi: 10.1109/LRA.2019.2963636.

[7] D. Blana, J. G. Hincapie, E. K. Chadwick, and R. F. Kirsch, "A musculoskeletal model of the upper extremity for use in the development of neuroprosthetic systems," *J. Biomech.*, vol. 41, no. 8, pp. 1714–1721, 2008, doi: 10.1016/j.jbiomech.2008.03.001.

[8] E. K. Chadwick, D. Blana, A. J. van den Bogert, and R. F. Kirsch, "A Real-Time, 3-D Musculoskeletal Model for Dynamic Simulation of Arm Movements," *IEEE Trans. Biomed. Eng.*, vol. 56, no. 4, pp. 941–948, Apr. 2009, doi: 10.1109/TBME.2008.2005946.

[9] M. Fadzli, A. Hanafusa, Y. Kubota, and D. Nishimori, "Preliminary Study on Muscle Force Estimation using Musculoskeletal Model for Upper Limb Rehabilitation with Assistive Device for Home Setting," *J. Phys. Conf. Ser.*, vol. 1372, p. 012023, Nov. 2019, doi: 10.1088/1742-6596/1372/1/012023.

[10] M. Mansouri and J. A. Reinbolt, "A platform for dynamic simulation and control of movement based on OpenSim and MATLAB," *J. Biomech.*, vol. 45, no. 8, pp. 1517–1521, May 2012, doi: 10.1016/j.jbiomech.2012.03.016.

[11] D. Blana, E. K. Chadwick, A. J. van den Bogert, and W. M. Murray, "Real-time simulation of hand motion for prosthesis control," *Comput. Methods Biomech. Biomed. Engin.*, vol. 20, no. 5, pp. 540–549, Apr. 2017, doi: 10.1080/10255842.2016.1255943.

[12] A. J. van den Bogert, D. Blana, and D. Heinrich, "Implicit methods for efficient musculoskeletal simulation and optimal control," *Procedia IUTAM*, vol. 2, no. 2011, pp. 297–316, Jan. 2011, doi: 10.1016/j.piutam.2011.04.027.

[13] A. Biess, D. G. Liebermann, and T. Flash, "A Computational Model for Redundant Human Three-Dimensional Pointing Movements: Integration of Independent Spatial and Temporal Motor Plans Simplifies Movement Dynamics," *J. Neurosci.*, vol. 27, no. 48, pp. 13045–13064, Nov. 2007, doi: 10.1523/JNEUROSCI.4334-06.2007.

[14] K. Nishikawa *et al.*, "Neuromechanics: an integrative approach for understanding motor control," *Integr. Comp. Biol.*, vol. 47, no. 1, pp. 16–54, May 2007, doi: 10.1093/icb/icm024.

[15] R. M. Enoka, *Neuromechanics of human movement*, Fifth edition. Champaign, IL: Human Kinetics, 2015.

[16] V. Gritsenko, R. L. Hardesty, M. T. Boots, and S. Yakovenko, "Biomechanical Constraints Underlying Motor Primitives Derived from the Musculoskeletal Anatomy of the Human Arm," *PLOS ONE*, vol. 11, no. 10, p. e0164050, Oct. 2016, doi: 10.1371/journal.pone.0164050.

[17] D. A. Winter, *Biomechanics and Motor Control of Human Movement*, 4th ed. Wiley, 2009.

[18] Kodak, "Ergonomics Design Philosophy," in *Kodak's Ergonomic Design for People at Work*, John Wiley & Sons, Ltd, 2007, pp. 1–98.

[19] E. V. Olesh, B. S. Pollard, and V. Gritsenko, "Gravitational and Dynamic Components of Muscle Torque Underlie Tonic and Phasic Muscle Activity during Goal-Directed Reaching," *Front. Hum. Neurosci.*, vol. 11, p. 474, 2017, doi: 10.3389/fnhum.2017.00474.

[20] D. W. Wagner *et al.*, "Consistency Among Musculoskeletal Models: Caveat Utilitor," *Ann. Biomed. Eng.*, vol. 41, no. 8, pp. 1787–1799, Aug. 2013, doi: 10.1007/s10439-013-0843-1.

[21] V. Gritsenko, N. I. Krouchev, and J. F. Kalaska, "Afferent Input, Efference Copy, Signal Noise, and Biases in Perception of Joint Angle During Active Versus Passive Elbow Movements," *J. Neurophysiol.*, vol. 98, no. 3, pp. 1140–1154, Sep. 2007, doi: 10.1152/jn.00162.2007.